VOLUME 89, NO. EM 1

PART 1

JOURNAL of the Engineering Mechanics Division

PROCEEDINGS OF THE

AMERICAN SOCIETY

OF CIVIL ENGINEERS

BASIC REQUIREMENTS FOR MANUSCRIPTS

Original papers and discussions of current papers should be submitted to the Manager of Technical Publications, ASCE. Authors should indicate the technical division to which the paper is referred. The final date on which a discussion should reach the Society is given as a footnote with each paper. Those who are planning to submit material will expedite the review and publication procedures by complying with the following basic requirements:

1. Titles must have a length not exceeding 50 characters and spaces.

2. A summary of approximately 50 words must accompany the paper; a 300-word synopsis must precede it, and a set of conclusions must end it.

3. The manuscript (an original ribbon copy and two duplicate copies) should be double-spaced on one side of 8½-inch by 11-inch paper. Three copies of all illustrations, tables, etc., must be included.

4. The author's full name, Society membership grade, and footnote reference stating present employment must appear on the first page of the paper.

5. Mathematics are retypeset from the copy that is submitted. Because of this, it is necessary that letters be drawn carefully, and that special symbols be properly identified. The letter symbols used should be defined where they first appear in the illustrations or in the text, and arranged alphabetically in an Appendix.

6. Tables should be typed (an original ribbon copy and two duplicate copies) on one side of 8½-inch by 11-inch paper. Specific illustration and explanation must be made in the text for each table.

7. Illustrations must be drawn in black ink on one side of 8½-inch by 11-inch paper. Because illustrations will be reproduced with a width of between 2 inches and 4½ inches, the lettering must be large enough to be legible in this width. Photographs should be submitted as glossy prints. Explanations and descriptions must be made within the text for each illustration.

8. The desirable average length of a paper is about 12,000 words and the absolute maximum is 15,000 words. As an approximation, each full page of typed text, table, or illustration is the equivalent of 500 words.

9. Technical papers intended for publication must be written in the third person.

10. The author should distinguish between a list of "Reading References" and a "Bibliography," which would encompass the subject of the paper.

Reprints from this Journal may be made on condition that the full title, name of author, name of publication, page reference, and date of publication by the Society are given. The Society is not responsible for any statement made or opinion expressed in its publications.

This Journal is published bimonthly by the American Society of Civil Engineers. Publication office is at 2500 South State Street, Ann Arbor, Michigan. Editorial and General Offices are at 33 West 39 Street, New York 18, New York. $4.00 of a member's dues are applied as a subscription to this Journal. Second class postage paid at Ann Arbor, Michigan.

The index for 1959 was published as ASCE Publication 1960-10 (list price $2.00); indexes for previous years are also available.

EDITED AS

Vol. 87 No. EM 3

Journal of the

ENGINEERING MECHANICS DIVISION

Proceedings of the American Society of Civil Engineers

ENGINEERING MECHANICS DIVISION
EXECUTIVE COMMITTEE
Egor P. Popov, Chairman; Bruce G. Johnston, Vice Chairman;
John W. Clark; Merit P. White; Edward Wenk, Jr., Secretary
Elmer K. Timby, Board Contact Member

COMMITTEE ON PUBLICATIONS
Bruce G. Johnston, Chairman; Hans H. Bleich; Jack E. Cermak;
Donald L. Dean; John E. Goldberg; William J. Hall; John D. Haltiwanger;
Herbert S. Suer; Joseph F. Throop

CONTENTS

June, 1961

Papers

Page

Attenuation of Stress Waves in Bi-Linear Materials
by Richard Skalak and Paul Weidlinger 1

Viscoelastic Winkler Foundation with Shear Interaction
by Arnold D. Kerr 13

Ultrasonic Evaluation of Reinforced Plastics
by Albert G. H. Dietz 31

(over)

Copyright 1961 by the American Society of Civil Engineers.

Note.—Part 2 of this Journal is the 1961-26 Newsletter of the Engineering Mechanics Division.

The three preceding issues of this Journal are dated December 1960, February 1961, and April 1961.

DISCUSSION

Page

White Noise Representation of Earthquakes, by G. N. Bycroft. (April, 1960. Prior discussion: August, 1960. Discussion closed.)
by G. N. Bycroft (closure) 47

Behavior of Buckled Rectangular Plates, by Manuel Stein. (April, 1960. Prior discussion: October, 1960. Discussion closed.)
by Manuel Stein (closure). 49

Behavior of Viscoelastic Plates in Bending, by George E. Mase. (June, 1960. Prior discussion: October, 1960. Discussion closed.)
by George E. Mase (closure) 51

Stresses Due to Thermal Gradients in Reactor Shieldings, by Melvin L. Baron and Mario G. Salvadori. (June, 1960. Prior discussion: December, 1960. Discussion closed.)
by Melvin L. Baron and Mario G. Salvadori (closure) 53

Underground Structures Subjected to Air Overpressure, by Ernest T. Selig, Keith E. McKee, and Eben Vey. (August, 1960. Prior discussion: February, 1961. Discussion closed.)
by Ernest T. Selig, Keith E. McKee, and Eben Vey (closure) 55

Arch Dam Analysis with an Analog Computer, by R. H. MacNeal. (August, 1960. Prior discussion: February, 1961. Discussion closed.)
by Raymond A. Hill 59

Dynamic Response of Beams Traversed by Two-Axle Loads, by Robert K. Wen. (October, 1960. Prior discussion: None. Discussion closed.)
by Enno Penno. 61

Bearing Capacity of Floating Ice Sheets, by G. G. Meyerhof. (October, 1960. Prior discussion: February, April, 1961. Discussion closed.)
by A. Assur. 63

Physical Metallurgy and Mechanical Properties of Materials: Brittle Fracture, by B. L. Averbach. (December, 1960. Prior discussion: None. Discussion closed.)
by H. L. Sujata and Hans Conrad. 67

Physical Metallurgy and Mechanical Properties of Materials: Fatigue of Structural Materials, by Horace J. Grover. (December, 1960. Prior discussion: None. Discussion closed.)
by S. K. Ghaswala 71

Page

Elasto-Plastic Analysis by Numerical Procedures, by Annabel L. Tong. (December, 1960. Prior discussion: April, 1961. Discussion closed.)
by Le-Wu Lu 75

Wind Induced Vibrations in Antenna Members, by William Weaver, Jr. (April, 1961. Prior discussion: None. Discussion closes: July 1, 1961.)
by Glenn B. Woodruff 81

Errata 83

Journal of the
ENGINEERING MECHANICS DIVISION
Proceedings of the American Society of Civil Engineers

ATTENUATION OF STRESS WAVES IN BI-LINEAR MATERIALS

By Richard Skalak,[1] M. ASCE, and Paul Weidlinger,[2] F. ASCE

SYNOPSIS

The attenuation of plane stress waves generated by a decaying surface pressure in a bi-linear medium is investigated, to obtain an approximate solution to the problem of a medium with a stress strain diagram of positive curvative. One-dimensional wave equations are derived, and it is demonstrated that, beyond a given distance from the surface, the intensity of the peak stress and particle velocity depends only on a single parameter. This result is of significance in establishing the relevant physical characteristics of granular soils which are subjected to high intensity nuclear surface blast pressures.

INTRODUCTION

Granular or porous materials, such as sand and/or certain types of rock, if subjected to high intensity compression, show a non-linear, strain-hardening behavior, characterized by a stress-strain curve (Fig. 1), of positive curvature, such that $\partial\sigma^2/\partial\epsilon^2 > 0$. On unloading, typically, a steeper path, such as AB in Fig. 1, is followed.

The attenuation of blast pressure is of major importance in investigations concerned with the effects of nuclear surface bursts, or underground structures

Note.—Discussion open until November 1, 1961. To extend the closing date one month, a written request must be filed with the Executive Secretary, ASCE. This paper is part of the copyrighted Journal of the Engineering Mechanics Division, Proceedings of the American Society of Civil Engineers, Vol. 87, No. EM 3, June, 1961.

[1] Assoc. Prof. of Civ. Engrg., Columbia Univ., New York, (on leave at Trinity College, Cambridge Univ., England).

[2] Cons. Engr., New York, N. Y.

and the detection of underground nuclear explosions. In order to discover the influence of the properties of the medium on these phenomena, the attenuation of stress waves as a function of the parameters which define the stress-strain relation must be established.

In the present paper, one-dimensional wave propagation with finite strain will be considered in a semi-infinite space, which on its free surface is sub-

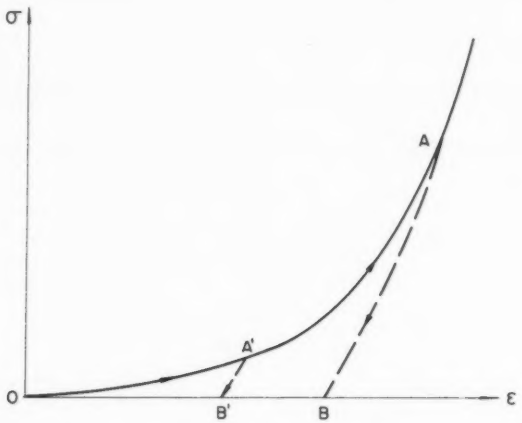

FIG. 1.—TYPICAL NON-LINEAR STRESS-STRAIN DIAGRAM

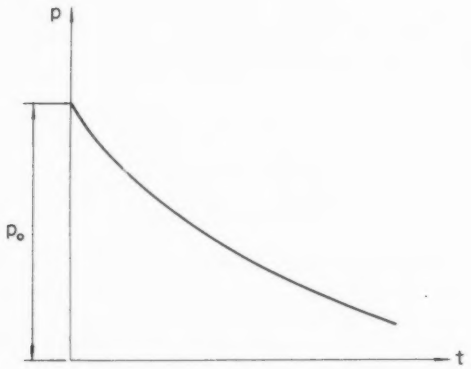

FIG. 2.—TYPICAL PRESSURE LOADING

jected to a pressure pulse of the form shown in Fig. 2. This problem can be solved by the method of characteristics,[3,4] for arbitrary stress-strain curves,

[3] "Mathematical Theory of Compressible Fluid Flow," by R. Von Mises, Academic Press, New York, 1958.

[4] "Supersonic Flow and Shock Waves," by R. Courant and K. O. Friedrich, Interscience Publisher, New York, 1958.

and numerical solutions have been obtained for the case of a constant boundary velocity.[5] Such procedure, however, requires extensive numerical integration and does not readily permit the assessment of the influence of the various parameters of the problem. More direct solutions to this problem are obtainable if a simplified bi-linear model of the stress-strain curve, such as shown in Fig. 3, is considered. On this stress-strain curve, up to the stress σ_c an

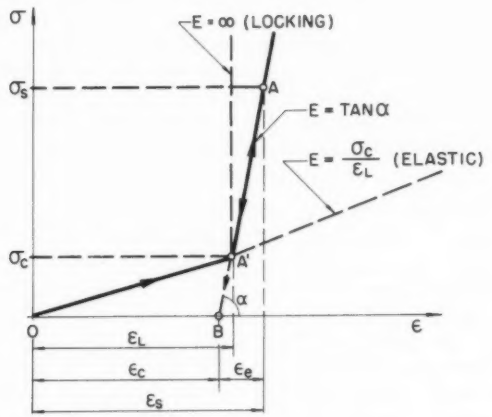

FIG. 3.—BI-LINEAR STRESS-STRAIN DIAGRAM

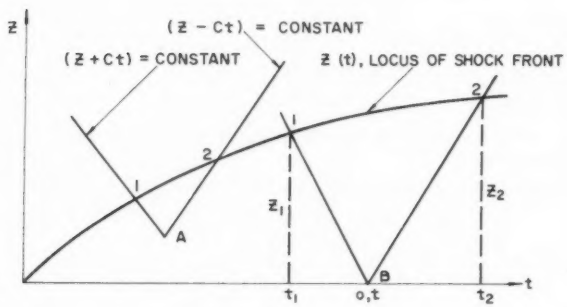

FIG. 4.—SPACE-TIME DIAGRAM

elastic behavior is postulated and the medium cannot be distinguished from an elastic material. If the medium is compressed beyond σ_c the path OA'A is followed, but unloading occurs on the line AB, resulting in a permanent strain ϵ_c. The medium is described by four parameters: the critical stress σ_c, the

5 "Propagation of Plane Waves in Granular Materials, Part I," by S. Katz and T. J. Ahrens, Rensselaer Polytechnic Inst., Report No. 1, Contract DA-20-115-509-ORD-1009, December, 1959.

permanent strain ϵ_c, and the slope α of the second branch of the curve, which defines the elastic modulus $E = \tan \alpha$, and if the initial density ρ of the medium is also given, the material is defined.

Considering now the limiting values of the parameters, the special case when $E = \infty$ is recognized, that is, the stress-strain diagram becomes that of a locking medium,[6] and the material becomes incompressible, when the strain $\epsilon_c = \epsilon_L$ is reached. The other limiting case is found when $\epsilon_c = 0$, which transforms the stress-strain diagram into that of an elastic medium with an elastic modulus $E = \sigma_c/\epsilon_L$. The main purpose of this paper is to investigate variations of the compressibility within the limits $\sigma_c/\epsilon_L \leq E \leq \infty$, and its effect on the attenuation of the peak pressures at various distances from the surface.

Notation.—The letter symbols adapted for use in this paper are defined where they first appear, in the illustrations or in the text, and are arranged alphabetically, for convenience of reference, in Appendix II.

WAVE EQUATIONS

Consider first the case in which σ_c in Fig. 3 is zero so that the stress-strain diagram consists of lines OB and BA. (Results for the case $\sigma_c > 0$ are easily obtained, as will be shown later, once the case $\sigma_c = 0$ is solved.)

The stress wave due to a loading of the form of Fig. 2 consists of a sharp shock front followed by a variable stress field with an essentially elastic behavior. The velocity of propagation of the shock front is

$$\dot{z}_S = \sqrt{\frac{\bar{E}}{\rho}} \quad \ldots\ldots\ldots\ldots\ldots\ldots \quad (1)$$

in which ρ is the initial density of the material and $\bar{E}$ is the secant modulus of elasticity, given by

$$\bar{E} = \frac{\sigma_S}{\epsilon_S} \quad \ldots\ldots\ldots\ldots\ldots\ldots\ldots \quad (2)$$

in which σ_S and ϵ_S are the normal vertical stress and strain immediately behind the shock front.

The particle velocity behind the shock wave is

$$\dot{u}_S = \frac{\sigma_S}{\rho \dot{z}_S} \quad \ldots\ldots\ldots\ldots\ldots\ldots\ldots \quad (3)$$

In terms of the modulus E of the line BA, Fig. 3, ϵ_S can be expressed by

$$\epsilon_S = \epsilon_c + \frac{\sigma_S}{E} = \epsilon_c + \frac{\sigma_S}{\rho c^2} \quad \ldots\ldots\ldots\ldots\ldots \quad (4)$$

in which

$$c^2 = \frac{E}{\rho} \quad \ldots\ldots\ldots\ldots\ldots\ldots\ldots \quad (5)$$

---

6 "Waves and Shocks in Locking and Dissipative Media," by M. G. Salvadori, R. Skalak, and P. Weidlinger, Proceedings, ASCE, Vol. 87, No. EM 2, April, 1960.

From Eq. 1 through 4 it follows that

$$\sigma_s = \rho \epsilon_c \dot{z}_s^2 \frac{1}{1 - \left(\frac{\dot{z}_s}{c}\right)^2} \quad \ldots\ldots\ldots\ldots\ldots \quad (6)$$

and

$$\dot{u}_s = \epsilon_c \dot{z}_s \frac{1}{1 - \left(\frac{\dot{z}_s}{c}\right)^2} \quad \ldots\ldots\ldots\ldots\ldots \quad (7)$$

The equation of motion of the material behind the shock wave is given by

$$\frac{\partial \sigma}{\partial z} = - \rho \frac{\partial \dot{u}}{\partial t} \quad \ldots\ldots\ldots\ldots\ldots\ldots \quad (8)$$

in Lagrangian coordinates, in which $u(z, t)$ is the displacement of particle at time t from its initial position, z. Compressive strain is defined by

$$\epsilon = - \frac{\partial u}{\partial z} \quad \ldots\ldots\ldots\ldots\ldots\ldots \quad (9)$$

Since ϵ_c is constant, Eq. 9 yields

$$\frac{\partial \left(\epsilon - \epsilon_c\right)}{\partial t} = - \frac{\partial \dot{u}}{\partial z} \quad \ldots\ldots\ldots\ldots\ldots \quad (10)$$

From Eq. 10 and the relation

$$\sigma = \left(\epsilon - \epsilon_c\right) E \quad \ldots\ldots\ldots\ldots\ldots \quad (11)$$

it follows that

$$\frac{1}{E} \frac{\partial \sigma}{\partial t} = - \frac{\partial \dot{u}}{\partial z} \quad \ldots\ldots\ldots\ldots\ldots\ldots \quad (12)$$

Eliminating $\dot{u}$ and σ in turn from Eq. 8 and 12 gives the one-dimensional wave equations

$$\frac{\partial^2 \sigma}{\partial t^2} = c^2 \frac{\partial^2 \sigma}{\partial z^2} \quad \ldots\ldots\ldots\ldots\ldots \quad (13)$$

and

$$\frac{\partial^2 \dot{u}}{\partial t^2} = c^2 \frac{\partial^2 \dot{u}}{\partial z^2} \quad \ldots\ldots\ldots\ldots\ldots \quad (14)$$

By virtue of Eq. 8, 12, 13, and 14, the field behind the shock wave can be expressed in the form

$$\sigma = f(z - c\,t) + g(z + c\,t) \quad \ldots\ldots\ldots\ldots \quad (15)$$

and

$$\dot{u} = \frac{c}{E}\left[f(z - c\,t) - g(z + c\,t)\right] \quad \ldots\ldots\ldots\ldots \quad (16)$$

In a space time plot, the locus of the shock front is a curve as shown in Fig. 4. Consider a general field point (z,t) such as point A in Fig. 4 and 2 points labeled 1 and 2 on the shock curve located by characteristics passing through the field point. By adding Eq. 15 and 16 for the point 2, it is found that

$$f(z_2 - c\,t_2) = \frac{1}{2}\sigma_2 + \frac{E}{2c}\dot{u}_2 \quad \ldots\ldots\ldots\ldots \quad (17)$$

and since (z - c t) is constant along the characteristic, it follows that for the field point (z, t)

$$f(z - c\,t) = \frac{1}{2}\sigma_2 + \frac{E}{2c}\dot{u}_2 \quad \ldots\ldots\ldots\ldots\ldots \quad (18)$$

Similarly, considering point 1, it is found that

$$g(z + c\,t) = \frac{1}{2}\sigma_1 - \frac{E}{2c}\dot{u}_1 \quad \ldots\ldots\ldots\ldots \quad (19)$$

and by substituting Eqs. 18 and 19 into Eqs. 15 and 16

$$\sigma = \frac{1}{2}(\sigma_1 + \sigma_2) - \frac{E}{2c}(\dot{u}_1 - \dot{u}_2) \quad \ldots\ldots\ldots \quad (20)$$

and

$$\dot{u} = \frac{1}{2}(\dot{u}_1 + \dot{u}_2) - \frac{c}{2E}(\sigma_1 - \sigma_2) \quad \ldots\ldots\ldots \quad (21)$$

are obtained.

If the locus of the shock wave, $z_s(t)$, is known, then σ_s and $\dot{u}_s$ are given by Eq. 6 and 7, and the remainder of the field can be found by Eq. 20 and 21. The solution is completed by establishing, $z_s(t)$, for a given surface pressure loading as follows:

Consider a field point which is on the surface z = 0 such as point B, Fig. 4. For this point the stress σ given by Eq. 20 is the applied pressure p at time t. By substituting the values for σ_1, σ_2 and $\dot{u}_1$, $\dot{u}_2$ from Eq. 6 and 7, an equation relating p, z_1 and z_2 is

$$\frac{2p}{\epsilon_c E} = \frac{\dot{z}_2}{c - \dot{z}_2} = \frac{\dot{z}_1}{c + \dot{z}_1} \quad \ldots\ldots\ldots\ldots\ldots \quad (22)$$

If the point B in Fig. 4 is assumed to move along the t axis, the pressure p(t) is the given surface pressure history. The heights shown in Fig. 4 labeled z_1 and z_2 and the times t_1 and t_2 may be also considered to be functions of t. The time t_1 is related to t by

$$t_1 = t - \frac{z_1}{c} \quad \ldots\ldots\ldots\ldots\ldots\ldots \quad (23)$$

Differentiating Eq. 23 with respect to t

$$\frac{dt_1}{dt} = 1 - \frac{1}{c}\frac{dz_1}{dt_1}\frac{dt_1}{dt} \quad \ldots\ldots\ldots\ldots\ldots \quad (24)$$

is obtained, in which the derivative $\frac{dz_1}{dt_1}$ is to be interpreted as $\dot{z}_1$ in Eq. 22.

Transforming Eq. 24 into the form

$$\frac{dt_1}{dt} = \frac{c}{c + \dot{z}_1} \quad \ldots\ldots\ldots\ldots\ldots\ldots \quad (25)$$

and defining z_1' by

$$z_1' = \frac{dz_1}{dt} = \frac{dz_1}{dt_1}\,\frac{dt_1}{dt} \quad \ldots\ldots\ldots\ldots\ldots \quad (26)$$

and using Eq. 25 the relation

$$\frac{z_1'}{c} = \frac{\frac{\dot{z}_1}{c}}{1 + \frac{\dot{z}_1}{c}} \quad \ldots\ldots\ldots\ldots\ldots\ldots \quad (27)$$

is obtained. Similarly from

$$t_2 = t + \frac{z_2}{c} \quad \ldots\ldots\ldots\ldots\ldots\ldots \quad (28)$$

it follows that

$$\frac{z_2'}{c} = \frac{\frac{\dot{z}_2}{c}}{1 - \frac{\dot{z}_2}{c}} \quad \ldots\ldots\ldots\ldots\ldots\ldots \quad (29)$$

in which

$$z_2' = \frac{dz_2}{dt} \quad \ldots\ldots\ldots\ldots\ldots\ldots \quad (30)$$

and

$$\dot{z}_2 = \frac{dz_2}{dt_2} \quad \ldots\ldots\ldots\ldots\ldots\ldots \quad (31)$$

Substituting Eqs. 27 and 29 into Eq. 22 yields

$$\frac{2c}{\epsilon_c E}\, p = z_2' - z_1' \quad \ldots\ldots\ldots\ldots\ldots \quad (32)$$

in which p is the function p(t) and the primes denote differentiation with respect to the variable t. Eq. 32 can be integrated with respect to t to yield the final equation

$$\frac{2c}{\epsilon_c E}\, I(t) = z_2 - z_1 \quad \ldots\ldots\ldots\ldots\ldots \quad (33)$$

in which I(t) is the impulse of p(t). The boundary conditions of Eq. 33 are $z_2 = z_1 = 0$ at $t = 0$.

Eq. 33 may be used to find the location z_2 of the shock front at time t_2 if the position z_1 at a time t_1 is known. To execute such computations it is neces-

sary to establish z_1 at some early time t as a starting point. For this purpose, a short time approximation is developed in Appendix, I.

NUMERICAL RESULTS

The magnitude of the front stress σ_s and particle velocity $\dot{u}_s$ (which are peak values experienced at a given depth), can be presented for all bi-linear materials in the domain $\sigma_c/\epsilon_c \leq E \leq \infty$ by a family of curves with the single parameter ϵ_e/ϵ_c as shown in Fig. 5 and Fig. 6. In the general case in which $\sigma_c > 0$, the peak stress and velocity propagate at the constant values σ_c and $\dot{u}_{sc}$ indefinitely after the stress at the front has decayed to this intensity. This behavior is due to the elastic action of the medium below the critical stress level and is indicated by a horizontal dotted line in Fig. 5 and 6, corresponding to some typical value σ_c and $\dot{u}_{sc}$ of the medium.

Numerical values are plotted in terms of a non-dimensional front stress σ_s/p_o for a decaying pressure load of the form

$$p(t) = p_o \exp\left(\frac{t}{t_o}\right) \quad \ldots\ldots\ldots\ldots\ldots \quad (34)$$

in which t_o is the relaxation time of the pressure. The location of the wave front, where the peak stress is experienced, is measured by the non-dimensional depth $z/(c_o t_o)$, in which

$$c_o = \left(\frac{p_o}{\rho \epsilon_c}\right)^{1/2} \quad \ldots\ldots\ldots\ldots\ldots \quad (35)$$

is the initial shock velocity of a locking medium corresponding to the limit $E \to \infty$. The non-dimensional particle velocity is defined by $\dot{u}_s/(c_o \epsilon_c)$, in which $c_o \epsilon_c$ is the initial particle velocity of a locking medium.

In the limiting case $\epsilon_e/\epsilon_c \to \infty$, which is reached by letting $\epsilon_c \to 0$, the medium responds elastically, which is shown by the constant peak stress and particle velocity at any depth. The other limit, corresponding to locking behavior is reached when the parameter $\epsilon_e/\epsilon_c \to 0$, which corresponds to the case $\epsilon_e = 0$.

As can be seen in Fig. 5 and 6, the stresses and particle velocities accociated with any value of the parameter ϵ_e/ϵ_c approach the curves representing the locking medium. The depth, beyond which the peak stress and peack velocity of bi-linear and locking medium becomes nearly coincidental corresponds to the time at which the first and principal rarefaction wave from the surface arrives at the shock front. If the surface pulse decays in a time of the order t_o, the depth of coincidence z_c is given by

$$z_c = \frac{c_o t_o}{\sqrt{1 + \frac{\epsilon_e}{\epsilon_c}} - \sqrt{\frac{\epsilon_e}{\epsilon_c}}} \quad \ldots\ldots\ldots\ldots\ldots \quad (36)$$

This approximate coincidence of peak values is of practical significance, since it demonstrates that stress attenuation beyond a certain, determinable depth,

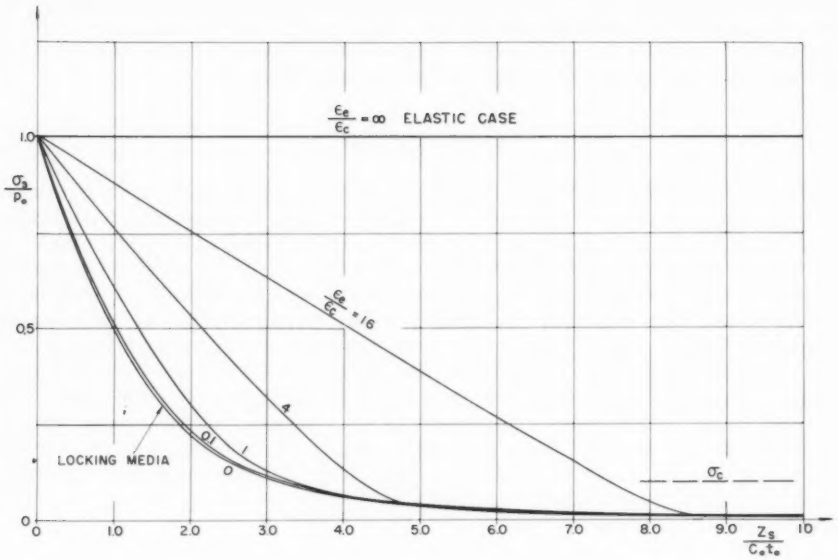

FIG. 5.—ATTENUATION OF PEAK STRESS

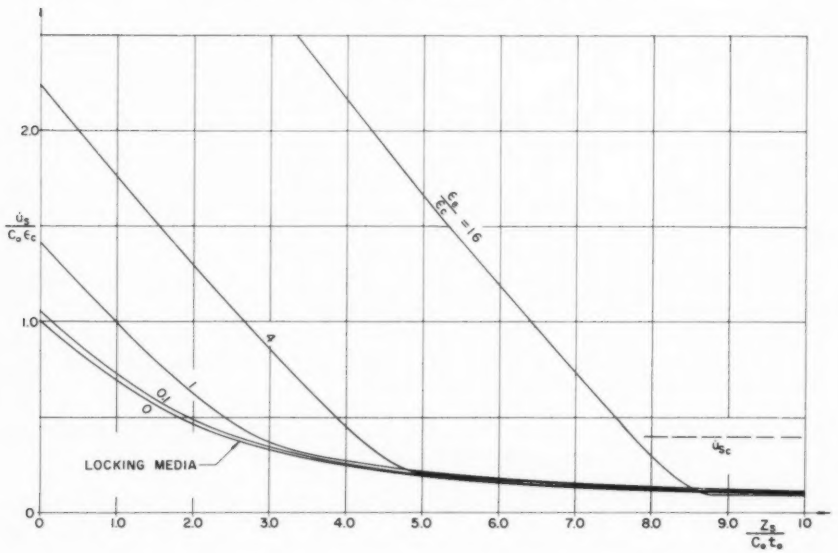

FIG. 6.—ATTENUATION OF PEAK PARTICLE VELOCITY

depends principally on the single parameter ϵ_c. Furthermore, in the case where the stress-strain diagram is a continuous curve, the decay of the peak stress and particle velocity can be estimated by a bi-linear approximation of the curve, which in turn reduces the problem to that of a single parameter, provided that the values of interest lie beyond the depth z_c.

CONCLUSIONS

The behavior of granular or porous materials such as sand, under confined compression is characterized by a non-linear strain hardening stress-strain curve, with large permanent strains on unloading. If the unloading occurs on a steep linear path, wave propagation problems in such media require extensive numerical work. Such materials, however, can be approximated by a bi-linear stress-strain diagram with resulting simplification in the mathematical and numerical treatment. This simplification provides means to estimate the influence of various mechanical properties of the medium on the attenuation of surface pressures, and of particle velocities. These investigations show that at early times attenuation is influenced by the character of the stress-strain relation, but at a greater depth, corresponding to later times, the behavior of various bi-linear materials becomes practically indistinguishable, resulting in further simplification of the problem.

ACKNOWLEDGMENTS

This paper is the result of investigations sponsored by the Air Research and Development Command, USAF.

APPENDIX I.

A surface pressure p(t), such as shown in Fig. 2 can be represented by a Taylor series

$$p(t) = p_o + p_1' t + \ldots \quad (37)$$

The values z_1 and z_2 may also be written in series form

$$z_1(t) = k_1 t + k_2 t^2 + \ldots \quad (38)$$

and

$$z_2(t) = m_1 t + m_2 t^2 + \ldots \quad (39)$$

Substituting Eqs. 37, 38, and 39 into Eq. 32 and equating coefficients of each power of t on the two sides of the equation yields

$$\frac{2c}{E\epsilon_c} = m_1 - k_1 \quad (40)$$

and

$$\frac{c}{E\epsilon_c} = m_2 - k_2 \quad (41)$$

etc . . .

The function $z_1(t)$ must also be such that at the appropriate time it is equal to the value of z_2 at an earlier time. This requirement may be written as

$$z_1(t) = z_2\left(t - \frac{2\,z_1\,(t)}{c}\right) \quad \ldots\ldots\ldots\ldots \quad (42)$$

in which all symbols in brackets represent independent variables of a function. Substituting Eq. 38 and 39 into Eq. 42 yields

$$k_1\,t + k_2\,t^2 + \ldots = m_1\left[t - \frac{2}{c}\left(k_1\,t + k_2\,t^2 + \ldots\right)\right] +$$

$$+ m_2\left[t - \frac{2}{c}\left(k_1\,t + k_2\,t^2 + \ldots\right)\right] +$$

$$+ \text{etc.} \quad \ldots\ldots\ldots\ldots\ldots\ldots \quad (43)$$

Equating coefficients of each power of t in Eq. 37 after expanding each term gives

$$k_1 = m_1\left(1 - \frac{2\,k_1}{c}\right) \quad \ldots\ldots\ldots\ldots\ldots \quad (44)$$

and

$$k_2 = -\,m_1\,\frac{2\,k_2}{c} + m_2\left(1 - \frac{2\,k_1}{c}\right)^2 \quad \ldots\ldots\ldots \quad (45)$$

Eq. 40 and 44 may be solved for k_1 and m_1

$$k_1 = \frac{c\,p_o}{E\,\epsilon_c}\left(-\,1 + \sqrt{1 + \frac{E\,\epsilon_c}{p_o}}\right) \quad \ldots\ldots\ldots \quad (46)$$

and

$$m_1 = \frac{c\,p_o}{E\,\epsilon_c}\left(1 + \sqrt{1 + \frac{E\,\epsilon_c}{p_o}}\right) \quad \ldots\ldots\ldots\ldots \quad (47)$$

Eqs. 41 and 45 may be solved for k_2 and m_2 considering k_1 and m_1 known

$$k_2 = \frac{c\,p'_o}{E\,\epsilon_c}\;\frac{k_1^3}{m_1^3 - k_1^3} \quad \ldots\ldots\ldots\ldots\ldots \quad (48)$$

and

$$m_2 = \frac{c\,p'_o}{E\,\epsilon_c}\;\frac{m_1^3}{m_1^3 - k_1^3} \quad \ldots\ldots\ldots\ldots\ldots \quad (49)$$

If the first two terms in Eq. 37 are considered adequate up to a time t, the corresponding value of z_1 is given by the first two terms of Eq. 38. The value of t_1 is given by Eq. 23. These values form a starting point for the computations using Eq. 33. After z_2 is established, by Eq. 33 for a given t, the value t_2 is found by Eq. 28. The computations proceed with these values of z_2 and t_2 of the previous step as the z_1, t_1 values for the next step.

In conducting numerical computations, it is convenient to use Eq. 32 as well as Eq. 33 so that the numerical results for $z_2(t)$ developed from Eq. 33 need not be differentiated numerically.

APPENDIX II. - NOTATION

c = acoustic velocity;

E = elastic modulus;

$\overline{E}$ = secant modulus;

$I(t)$ = impulse of surface pressure;

k = constant;

m = constant;

P_o = initial value of surface pressure;

$p(t)$ = surface pressure;

t = time;

t_o = relaxation time;

z_s = location of shock front;

z_s = shock velocity;

ϵ = strain;

ρ = density; and

σ = stress.

Journal of the
ENGINEERING MECHANICS DIVISION
Proceedings of the American Society of Civil Engineers

VISCOELASTIC WINKLER FOUNDATION WITH SHEAR INTERACTIONS

By Arnold D. Kerr[1]

SYNOPSIS

The concept of the Pasternak-foundation, consisting of the Winkler-foundation with shear interactions, is extended herein to the case of visco-elastic behavior. The D. E. for the vertical surface displacements w due to creep is formulated and solutions for several loading cases are worked out. In addition to the elastic constant two material parameters enter the analysis: The viscosity parameter μ related to the shear deformations and η a visco-compressibility parameter of the vertical foundation elements. A procedure to determine these parameters is suggested. The application of this analysis to the creep behavior of snow foundations is examined.

INTRODUCTION AND STATEMENT OF THE PROBLEM

It was observed in the field as well as from experiments that materials such as compacted snow masses or certain frozen grounds show large creep deformations when subjected to loads of long duration. One of the main characteristics is that these deformations vary with time and by far exceed the elastic displacements.

Several papers have appeared on the subject of beams or plates on a visco-elastic foundation.[2,3] In these papers the Winkler assumption was ex-

Note.—Discussion open until November 1, 1961. To extend the closing date one month, a written request must be filed with the Executive Secretary, ASCE. This paper is part of the copyrighted Journal of the Engineering Mechanics Division, Proceedings of the American Society of Civil Engineers, Vol. 87, No. EM 3, June, 1961.

1 Asst. Prof. of Aeronautics, New York Univ., New York, and Consultant to Snow Ice and Permafrost Research Establishment, Corps of Engrs., U. S. Army.

2 "The Infinite Elastic Beam on a Linear Viscoelastic Foundation," by A. M. Freudenthal and H. G. Lorsch, Proc. Paper No. 1158, ASCE, Vol. 83, No. EM 1, January, 1957.

3 "Flexible Surfaces on Viscoelastic Subgrades," by B. C. Hoskin and E. H. Lee, Proceedings, ASCE, Vol. 85, No. EM 4, October, 1959.

tended by adding linear viscous elements to the elastic springs in parallel or series arrangements (Maxwell model, Kelvin model, or their combination). No interaction between the particular foundation elements was assumed.

Experiments indicate that compacted snow as well as granular media does not behave like a Winkler-type foundation consisting of independent vertical

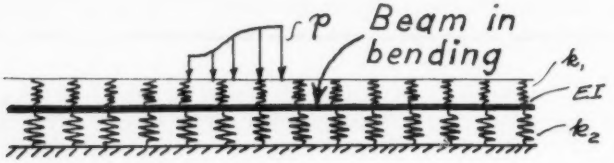

FIG. 1.—FOUNDATION MODEL ACCORDING TO HETÉNYI

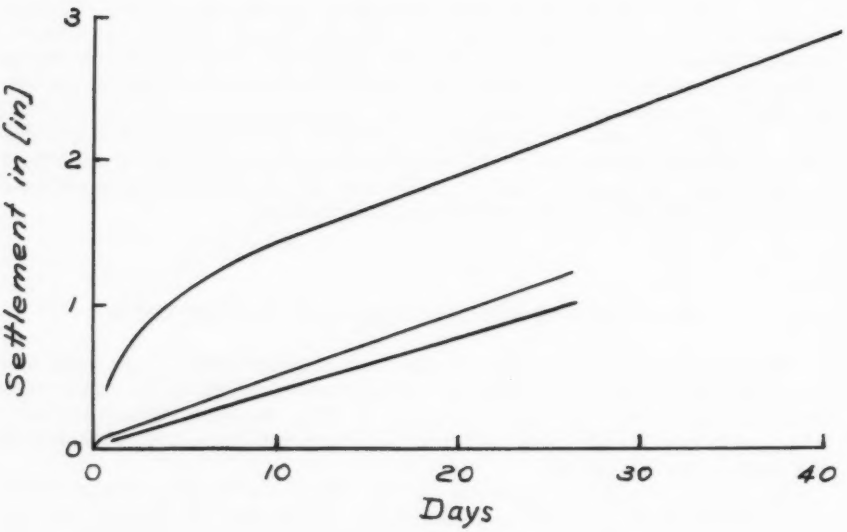

FIG. 2.—FOOTING LOAD TEST ON A SNOW BASE. TIME-SETTLEMENT GRAPHS (SPIRE, 1959)

elements nor like an isotropic continuum but somewhere in between. It was found namely that deformations due to outside loads are confined to the vicinity of the loaded region. To bridge the gap between the two extreme foundation models, M. Hetényi,[4] F. ASCE, suggested imbedding a continuous

4 "Beams on Elastic Foundations," by M. Hetényi, The University of Michigan Press, Ann Arbor, Mich., 1946.

elastic beam in the material of the elastic foundation as shown in Fig. 1 and assumed that the beam deforms in bending only. P. L. Pasternak[5] treated the problem by assuming the existence of shear interactions between the spring elements. This approach is equivalent to the assumption of a beam or plate that rests on a spring foundation and deforms only due to transverse shear. With this assumption the foundation is characterized by two constants; one representing the elastic foundation, the other the intensity of elastic shear interaction. From the point of view of the mechanism of deformation of com-

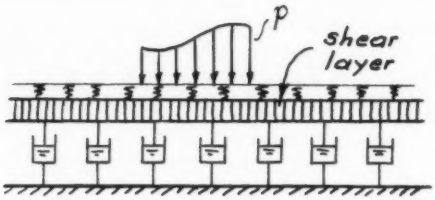

FIG. 3.—FOUNDATION MODEL USED HEREIN

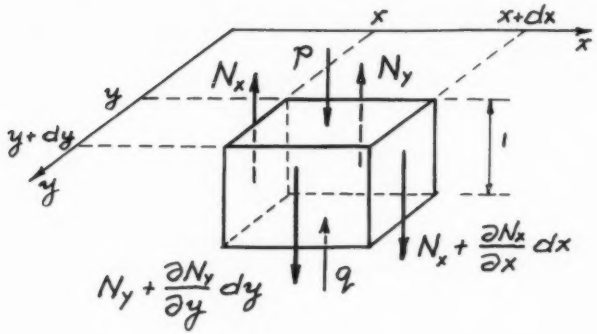

FIG. 4.—FORCES ACTING ON A SHEAR LAYER ELEMENT

pacted snow masses, it seems that the Pasternak-foundation is a very suitable model.

Herein the concept of the Pasternak-foundation is extended to the case of viscoelastic deformations, and the behavior of the foundation surface subjected to different load situations is studied as a function of time. Results of footing load tests performed on a snow base by the Snow Ice and Permafrost Research Establishment, Corps of Engineers, U. S. Army (SIPRE) in Greenland (1959) are shown in Fig. 2. It can be seen that, after a relatively short initial period,

5 "Osnovy Novogo Metodo Rascheta Rundamentov na Uprugom Osnovani pri Pomoshchi Dvuch Koefficientov Posteli," by P. L. Pasternak, Gos. Izd. Lit. po Stroitelstvu i Architekture, Moscow, 1954.

a linear time displacement relationship exists. (It seems that one prerequisite is that the foundation dimensions should be large in comparison to the dimensions of the loaded area.) This suggests the possibility of assuming Newton's law for the viscous behavior, that yields a linear time displacement relationship. Because the elastic deformations, that take place immediately after the load application, are very small as compared to the creep deformations, it seems justified to assume a foundation as shown in Fig. 3. The total deflection is then

$$w_{total} = w_{elastic} + w \quad \ldots\ldots\ldots\ldots\ldots\ldots \quad (1)$$

Whereas $w_{elastic}$ is obtainable in the usual manner, the following sections will deal with the deflections w due to creep.

Notation.—The letter symbols adopted for use in this paper are defined where they first appear, in the illustrations or in the text, and are arranged alphabetically, for convenience of reference, in Appendix I.

FORMULATION OF THE PROBLEM

The investigated semi-infinite medium is represented by a layer of unit thickness, consisting of incompressible vertical elements, that deforms by transverse shear only, and that rests on closely spaced linear viscous elements as shown in Fig. 3.

The vertical equilibrium of a "shear layer" is considered as parallelepiped cut out by the vertical surfaces x, $x+dx$, y and $y+dy$ as shown in Fig. 4. Because, for the cases under consideration, the movements of the foundation surface are very slow, the inertia terms are neglected.

The equilibrium equation is

$$\frac{\partial N_x}{\partial x} + \frac{\partial N_y}{\partial y} + p - q = 0 \quad \ldots\ldots\ldots\ldots\ldots\ldots \quad (2)$$

Assuming that foundation material is homogeneous and isotropic then according to Newton's law of viscosity

$$N_x = \mu \frac{\partial^2 w}{\partial x\, \partial t} \quad \ldots\ldots\ldots\ldots\ldots\ldots \quad (3)$$

$$N_y = \mu \frac{\partial^2 w}{\partial y\, \partial t} \quad \ldots\ldots\ldots\ldots\ldots\ldots \quad (4)$$

and

$$q = \eta \frac{\partial w}{\partial t} \quad \ldots\ldots\ldots\ldots\ldots\ldots \quad (5)$$

in which $\frac{\partial w}{\partial t}$ is the downward velocity of the foundation surface.

It should be noted that two constants of the foundation material enter the analysis: A viscosity coefficient μ related to the shear deformation of vertical foundation elements and η, a visco-compressibility coefficient. Substituting Eqs. 3, 4, and 5 into Eq. 2 yields

$$\mu \left(\frac{\partial^3 w}{\partial x^2\, \partial t} + \frac{\partial^3 w}{\partial y^2\, \partial t} \right) - \eta \frac{\partial w}{\partial t} + p(x, y, t) = 0 \quad \ldots\ldots\ldots \quad (6a)$$

If the load is time independent, p = p(x, y), after differentiation of Eq. 6 with respect to t it reduces to

$$\frac{\partial^2}{\partial t^2}\left(\frac{\partial^2}{\partial x^2} + \frac{\partial^2}{\partial y^2} - \lambda^2\right) w = 0 \quad \ldots\ldots\ldots\ldots (6b)$$

or

$$\frac{\partial^2}{\partial t^2}\left(\Delta - \lambda^2\right) w = 0 \quad \ldots\ldots\ldots\ldots\ldots\ldots (7)$$

in which Δ is the Laplacian and $\lambda^2 = \frac{\eta}{\mu}$.

Eq. 7 is the D. E. for the vertical displacement of the foundation surface. According to the assumptions made, the displacements in the x-y plane are zero. It should also be noted that no restrictions were imposed upon the magnitude of w to obtain Eq. 7 as a linear equation.

Eq. 7 can also be obtained going out from the equations of a continuum, setting the stresses

$$\delta_x = \delta_y = \tau_{xy} = 0 \quad \ldots\ldots\ldots\ldots\ldots\ldots (8)$$

as was done by E. Reissner[6] who formulated the problem of an elastic plate resting on a visco-elastic foundation of the Kelvin type with shear interactions.

In the following, solutions of Eq. 7 are evolved for a number of practical loading cases in order to facilitate proof of the applicability of the preceding theory for different foundation materials through a series of tests in the field, as well as for later use in engineering praxis.

LINE LOAD $\overline{P}$ ALONG THE y AXIS

For the case of the line load $\overline{P}$ along the y axis, w = w(x, t) and Eq. 7 reduces to

$$\frac{\partial^2}{\partial t^2}\left(\frac{\partial^2}{\partial x^2} - \lambda^2\right) w = 0 \quad \ldots\ldots\ldots\ldots\ldots\ldots (9)$$

Assuming the solution in the form w = X(x) T(t), Eq. 9 will be satisfied if

$$\frac{d^2T}{dt^2} = 0 \quad \ldots\ldots\ldots\ldots\ldots\ldots (10a)$$

and

$$\frac{d^2X}{dx^2} - \lambda^2 X = 0 \quad \ldots\ldots\ldots\ldots\ldots\ldots (10b)$$

Thus

$$w(x, t) = \left(C_1 + C_2 t\right)\left(Ae^{\lambda x} + Be^{-\lambda x}\right) \quad \ldots\ldots\ldots\ldots (11)$$

The deflection w is expected to vanish at $x = \infty$, so that A = 0, and because for t = 0 the deflections due to creep are zero it follows that $C_1 = 0$. With $C_2 B = C$,

$$w(x, t) = C\, t\, e^{-\lambda x} \qquad x \geq 0 \quad \ldots\ldots\ldots\ldots\ldots (12)$$

---

6 "A Note on Deflection of Plates on a Viscoelastic Foundation," by E. Reissner, Journal of Applied Mechanics, March, 1958.

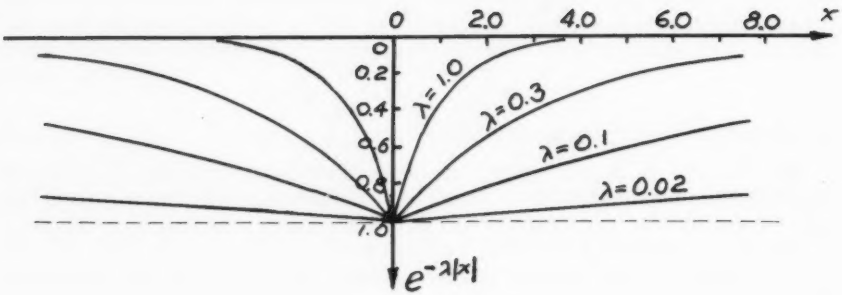

FIG. 5.—DEFLECTION FUNCTION DUE TO A LINE LOAD $\bar{P}$ FOR DIFFERENT VALUES OF λ

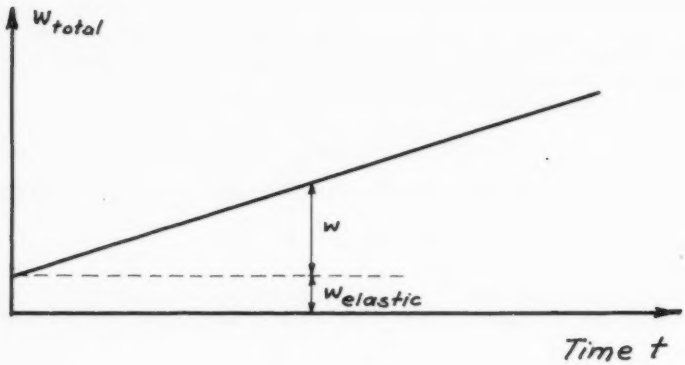

FIG. 6.—TIME-DISPLACEMENT GRAPH

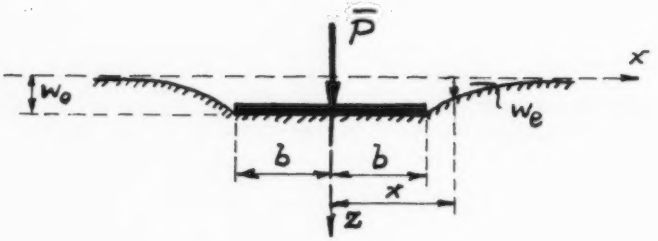

FIG. 7.—A SECTION THROUGH THE RIGID STRIP AND BASE

The constant C is determined from the condition of vertical equilibrium for any time t.

$$\overline{P} - 2 \int_0^\infty q \, dx = 0 \quad \ldots\ldots\ldots\ldots\ldots\ldots (13)$$

With

$$q = \eta \frac{\partial w}{\partial t} = \eta C e^{-\lambda x} \quad \ldots\ldots\ldots\ldots\ldots\ldots (14)$$

then

$$C = \frac{\lambda \overline{P}}{2 \eta} \quad \ldots\ldots\ldots\ldots\ldots\ldots (15)$$

and

$$w(x, t) = \frac{\overline{P} \lambda}{2} \left(\frac{1}{\eta} t\right) e^{-\lambda x} \qquad x \geq 0 \quad \ldots\ldots\ldots\ldots (16)$$

Thus the surface of the medium will deform according to an exponential function (see Fig. 5) and the time deflection relation is linear and will be of the nature shown in Fig. 6. The discontinuity in slope along the line of application of the "concentrated" line load is a consequence of the assumptions made and will disappear once the line load is replaced by one of finite width as done in the following.

UNIFORMLY DISTRIBUTED LOAD p IN THE INTERVAL -b = x = +b

The solution for loading case of the uniformly distributed load p in the interval -b = x = +b is obtained from the previous result setting $\overline{P} = p \, d\xi$ and integrating from -b to +b. The deflections outside the loaded region $x \geq b$ are

$$w_e = p \frac{t}{\eta} \sinh(\lambda b) e^{-\lambda x} \quad \ldots\ldots\ldots\ldots\ldots\ldots (17)$$

and the deflections inside the loaded region $-b \leq x \leq b$ are

$$w_i = p \frac{t}{\eta} \left[1 - e^{-\lambda b} \cosh(\lambda x)\right] \quad \ldots\ldots\ldots\ldots\ldots\ldots (18)$$

FOUNDATION LOADED CENTRALLY BY A RIGID STRIP

A section through the rigid strip and base of a foundation loaded by the rigid strip is shown in Fig. 7. Under the strip, $-b < x < +b$, the deflection w_0 is constant. The corresponding vertical pressure is, according to Eq. 5,

$$q_0 = \eta \left(\frac{dw_0}{dt}\right) \quad \ldots\ldots\ldots\ldots\ldots\ldots (19)$$

in which dw_0/dt is the downward velocity of the strip.

The deflection surface for $x \geq b$ is determined from the continuity condition that at a time t, w(x, t) will pass through $w_0(b, t)$ for any λ. Thus, according to Eq. 12, at x = b

$$w_0(b, t) = C t e^{-\lambda b} \quad \ldots\ldots\ldots\ldots\ldots\ldots (20)$$

It follows that $C = \frac{w_0}{t} e^{\lambda b}$. Substituting C in Eq. 12

$$w_e(x, t) = w_0 e^{-\lambda (x - b)} \qquad x \geq b \quad \ldots\ldots\ldots\ldots (21)$$

and

$$q_e = \eta \left(\frac{dw_0}{dt}\right) e^{-\lambda (x - b)} \quad \ldots\ldots\ldots\ldots\ldots\ldots (22)$$

Substituting in the vertical equilibrium equation (per unit length of strip)

$$\overline{P} - q_0\ 2b + 2 \int_b^\infty q_e\ dx = 0 \quad \ldots\ldots\ldots\ldots (23)$$

Eqs. 19 and 22, after integrating, it follows that

$$\overline{P} = 2\eta \left(\frac{dw_0}{dt}\right) \left(b + \frac{1}{\lambda}\right) \quad \ldots\ldots\ldots\ldots\ldots\ldots (24)$$

or

$$\left(\frac{dw_0}{dt}\right) = \frac{\overline{P}}{2\ \eta(\lambda\ b + 1)} \quad \ldots\ldots\ldots\ldots\ldots\ldots (25)$$

This is the velocity of the downward motion of the rigid strip of width 2b. The corresponding vertical displacement is

$$w_0\ (t) = \frac{\lambda\ \overline{P}}{2\ \eta(\lambda\ b + 1)}\ t \quad \ldots\ldots\ldots\ldots\ldots\ldots (26)$$

if it is assumed that at t = 0 the creep deformation starts.

Because the deflection w_0 under the strip $-b < x < +b$ is constant, no shear forces occur in this region. The pressure distribution under the strip is

$$q_i = \eta \left(\frac{dw_0}{dt}\right) \quad \ldots\ldots\ldots\ldots\ldots\ldots (18)$$

and because of equilibrium (Eq. 24) two line loads

$$\overline{q} = \frac{\eta}{\lambda} \left(\frac{dw_0}{dt}\right) \quad \ldots\ldots\ldots\ldots\ldots\ldots (27)$$

per unit length of strip act along the edges $x = \pm b$, as shown in Fig. 8.

RIGID STRIP SUBJECTED TO A CENTRAL LOAD AND MOMENT

Because of the linearity of the problem involved in the case of a rigid strip subjected to a central load and moment the vertical displacements can be split into a downward translatory motion and a rotation as shown in Fig. 9. Each part can be treated separately and then the displacements added.

A condition is that the total load should not create tension in the contact area of the strip and foundation, that is

$$\frac{M}{P} = e \leq \frac{b}{3} \quad \ldots\ldots\ldots\ldots\ldots\ldots (28)$$

It is assumed that the load P and the moment M are time independent.

The case of the rigid strip exerting a central load was treated previously. The problem of the rigid strip subjected to a moment M will now be solved.

With the notation as shown in Fig. 10

$$w_i\ (t) = \alpha_o\ (t)\ x \quad \ldots\ldots\ldots\ldots\ldots\ldots (29a)$$

$$q_i = \eta\ x \left(\frac{d\alpha_o}{dt}\right) = \eta\ \omega_o\ x \quad \ldots\ldots\ldots\ldots\ldots\ldots (29b)$$

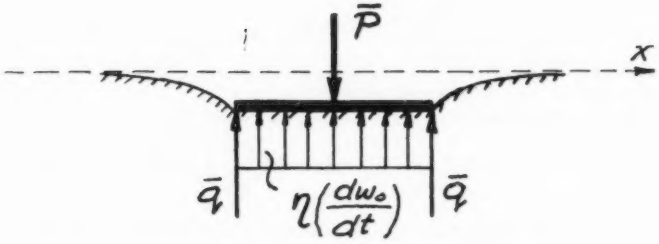

FIG. 8.—PRESSURE DISTRIBUTION UNDER THE STRIP

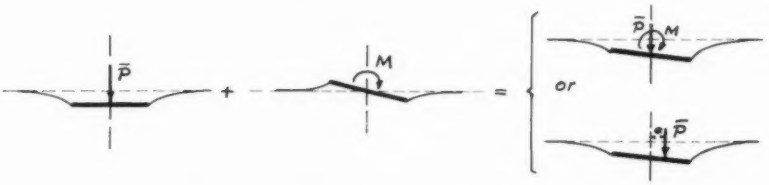

FIG. 9.—SUPERPOSITION OF EFFECTS DUE TO P AND M

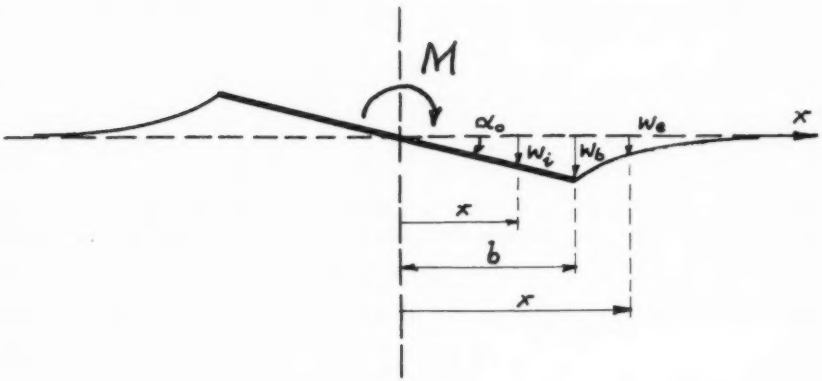

FIG. 10.—A SECTION THROUGH A RIGID STRIP AND BASE SUBJECTED TO A MOMENT

for $-b \leq x \leq b$ and

$$w_e = w_b\, e^{-\lambda (x - b)} = \alpha_o\, b\, e^{-\lambda (x - b)} \quad \ldots\ldots\ldots (30a)$$

$$q_e = \eta \left(\frac{dw_b}{dt}\right) e^{-\lambda (x - b)} = \eta\, b\, \omega_o\, e^{-\lambda (x - b)} \quad \ldots\ldots\ldots (30b)$$

for $x \geq b$ in which ω_o is angular velocity.

Moment equilibrium about $x = 0$ requires that

$$M - 2 \int_o^b q_i\, x\, dx - 2 \int_b^\infty q_e\, x\, dx = 0 \quad \ldots\ldots\ldots (31)$$

Substituting Eqs. 29b and 30b into Eq. 31 and integrating it yields

$$M = \frac{2}{3} \eta\, \omega \frac{b}{\lambda^2} \left[(\lambda\, b)^2 - 3\,(\lambda\, b) - 3\right] \ldots\ldots\ldots (32)$$

and

$$\omega_o = \frac{3}{2} \left\{ \frac{\lambda^2\, M}{\eta\, b \left[(\lambda\, b)^2 - 3(\lambda\, b) - 3\right]} \right\} \ldots\ldots\ldots (33)$$

The angle of rotation α_o at a time t is then

$$\alpha_o = \frac{3}{2} \left\{ \frac{\lambda^2\, M\, t}{\eta\, b \left[(\lambda\, b)^2 - 3(\lambda\, b) - 3\right]} \right\} \ldots\ldots\ldots (34)$$

if it is assumed that at $t = 0$ the creep deformation starts.

FOUNDATION SUBJECTED TO A CONCENTRATED LOAD, P

A foundation subjected to a concentrated load P is an axially symmetrical case for which the Laplacian is of the form

$$\Delta = \left(\frac{\partial^2}{\partial r^2} + \frac{1}{r} \frac{\partial}{\partial r}\right) \quad \ldots\ldots\ldots (35)$$

The solution of Eq. 7 is now

$$w(r, t) = \left(C_1 + C_2 t\right) \left[A\, I_o\, (\lambda\, r) + B\, K_o\, (\lambda\, r)\right] \quad \ldots\ldots\ldots (36)$$

Because w is expected to be zero at infinity, it follows $A = 0$. For $t = 0$ the deformations due to creep are zero, thus $C_1 = 0$. Letting $C_2\, B = C$ yields

$$w = C\, t\, K_o\, (\lambda\, r) \quad \ldots\ldots\ldots (37)$$

The constant C is determined from the vertical equilibrium condition. With

$$q = \eta \frac{\partial w}{\partial t} = \eta\, C\, K_o\, (\lambda\, r) \quad \ldots\ldots\ldots (38)$$

$$P = \int_o^{2\pi} \int_o^\infty q\, r\, dr\, dt = 2\, \pi\, \eta\, C \int_o^\infty r\, K_o\, (\lambda\, r)\, dr = 2\, \pi\, C \frac{\eta}{\lambda^2} \ldots (39)$$

and

$$C = \frac{\lambda^2\, P}{2\, \pi\, \eta} \quad \ldots\ldots\ldots (40)$$

Hence

$$w(r, t) = \frac{\lambda^2 P}{2 \pi} \frac{t}{\eta} K_0(\lambda r) \quad \ldots\ldots\ldots\ldots\ldots (41)$$

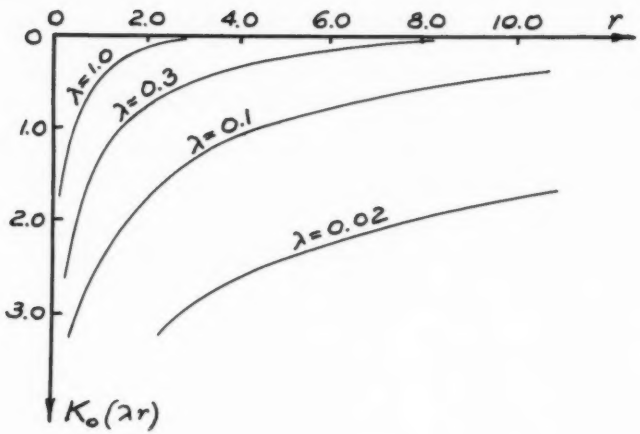

FIG. 11.—DEFLECTION FUNCTION DUE TO A CONCENTRATED LOAD P FOR DIFFERENT VALUES OF λ

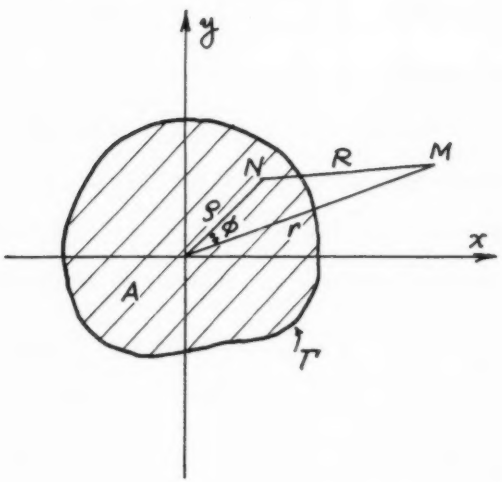

FIG. 12

The graphical representation of the deflection function for different values of λ is shown in Fig. 11. Eq. 41 contains a logarithmic singularity at r = 0. The

deflection will be finite, however, once the load is assumed distributed over a finite area, as shown in the following section.

FOUNDATION SUBJECTED TO A UNIFORMLY DISTRIBUTED LOAD INSIDE A CIRCULAR AREA

For the case of a foundation subjected to a uniformly distributed load inside a circular area, consider an area A of the surface subjected to an arbitrary load distribution as shown in Fig. 12.

The deflections at an arbitrary point M caused by a load element at N

$$dP = q\, dA = q(\rho, \phi)\, \rho\, d\rho\, d\phi \quad \ldots\ldots\ldots\ldots (42)$$

is then

$$dw = \frac{\lambda^2}{2\pi} \frac{t}{\eta} K_o(\lambda R)\, q(\rho, \phi)\, \rho\, d\rho\, d\phi \quad \ldots\ldots\ldots (43a)$$

and due to the entire distributed load

$$w = \frac{\lambda^2}{2\pi} \frac{t}{\eta} \int\int_A q(\rho, \phi) K_o(\lambda R)\, \rho\, d\rho\, d\phi \quad \ldots\ldots\ldots (43b)$$

in which

$$R = r^2 + \rho^2 - 2 r \rho \cos\phi \quad \ldots\ldots\ldots\ldots\ldots (44)$$

and the integration is to be performed over the loaded region A. Assuming q is a constant distributed over a circular area of radius a with center at r = 0 yields

$$w_e(r, t) = \frac{\lambda^2 q}{2\pi} \frac{t}{\eta} \int_{\phi=0}^{2\pi} \int_{\rho=0}^{a} \rho\, K_o(\lambda R)\, d\rho\, d\phi \quad \ldots\ldots (45)$$

Using Eq. 77 (see Appendix II) Eq. 45 reduces to

$$w_e(r, t) = \lambda^2 q \frac{t}{\eta} K_o(\lambda r) \int_o^a \rho\, I_o(\lambda \rho)\, d\rho \quad \ldots\ldots\ldots (46)$$

and applying formula 835.3 given by H. B. Dwight[7]

$$w_e(r, t) = q \frac{t}{\eta} (\lambda a) I_1(\lambda a) K_o(\lambda r) \qquad \text{for } r \geq a \quad \ldots\ldots\ldots (47)$$

The deflection expression for any point inside the loaded region is (see Fig. 13)

$$w_i(r, t) = \frac{\lambda^2 q}{2\pi} \frac{t}{\eta} \left(\underbrace{\int_o^{2\pi} \int_o^{r} \rho\, K_o(\lambda R)\, d\rho\, d\phi}_{r > \rho} + \underbrace{\int_o^{2\lambda} \int_r^{a} \rho\, K_o(\lambda R)\, d\rho\, d\phi}_{r < \rho} \right) \quad \ldots\ldots (48)$$

Applying Eq. 77 (see Appendix II) to the first integral expression and Eq. 78 (see Appendix II) to the second one yields

$$w_i(r, t) = \lambda^2 q \frac{t}{\eta} \left[K_o(\lambda r) \int_o^r \rho\, I_o(\lambda \rho)\, d\rho + I_o(\lambda r) \int_r^a \rho\, K_o(\lambda \rho)\, d\rho \right] \quad \ldots\ldots (49)$$

---

7 "Tables of Integrals and Other Mathematical Data," by H. B. Dwight, Revised Edition, The McMillan Co., New York, 1947.

Using formulas 835.3 and 835.5 given by Dwight[7] and with the identity

$$I_o(\lambda r) K_1(\lambda r) + K_o(\lambda r) I_1(\lambda r) = \frac{1}{(\lambda r)} \quad \ldots\ldots\ldots (50)$$

it follows that

$$w_i(r,t) = q \frac{t}{\eta} \left[1 - (\lambda a) K_1(\lambda a) I_o(\lambda r)\right] \qquad \text{for } r \leq a \quad \ldots (51)$$

At $r = 0$

$$w_i(o,t) = q \frac{t}{\eta} \left[1 - (\lambda a) K_1(\lambda a)\right] \ldots\ldots\ldots\ldots (52)$$

FOUNDATION LOADED CENTRALLY BY A CIRCULAR RIGID PLATE

A section through the rigid plate and base of a foundation loaded centrally by a circular rigid plate at a time t is as shown in Fig. 7, replacing b by radius a and x by r. By an argument similar to that previously given under the section headed "Foundation Loaded Centrally by a Rigid Strip," denoting for any t the corresponding vertical displacement of the plate by $w_o(t)$, the deflections in the region $r \geq a$ are

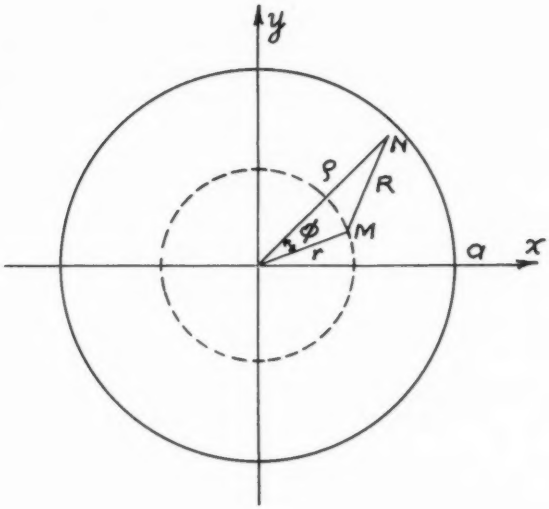

FIG. 13

$$w_e = w_o \frac{K_o(\lambda r)}{K_o(\lambda a)} \ldots\ldots\ldots\ldots\ldots\ldots (53)$$

and

$$q_i = \eta \left(\frac{\partial w_o}{\partial t}\right) \qquad r \leq a \ldots\ldots\ldots\ldots\ldots (54a)$$

and

$$q_e = \eta \left(\frac{\partial w_o}{\partial t}\right) \frac{K_o(\lambda r)}{K_o(\lambda a)} \qquad r \geq a \quad \ldots\ldots\ldots (54b)$$

Vertical equilibrium requires that

$$P - \int_0^{2\pi} \int_0^{a} q_o r \, dr \, d\theta - \int_0^{2\pi} \int_a^{\infty} q_e \, r \, dr \, d\theta = 0 \quad \ldots\ldots\ldots (55)$$

Substituting the expressions for q into Eq. 55 and integrating yields

$$P = \pi \eta a^2 \left(\frac{dw_o}{dt}\right)\left[1 + 2 \frac{K_1(\lambda a)}{(\lambda a) K_o(\lambda a)}\right] \quad \ldots\ldots\ldots (56)$$

and

$$\left(\frac{dw_o}{dt}\right) = \frac{\lambda^2 K_o(\lambda a) P}{\pi \eta (\lambda a)\left[(\lambda a) K_o(\lambda a) + 2 K_1(\lambda a)\right]} \quad \ldots\ldots\ldots (57)$$

This is the sinking velocity of the rigid plate. The corresponding vertical displacement at time t is

$$w_o(t) = \frac{\lambda^2 K_o(\lambda a) P}{\pi (\lambda a)\left[(\lambda a) K_o(\lambda a) + 2 K_1(\lambda a)\right]} \frac{t}{\eta} \quad \ldots\ldots (58)$$

if it is assumed that at t = 0 the creep deformation starts.

The corresponding vertical pressure distribution in the contact area of plate and base is similar in nature to that described in the section dealing with a foundation loaded centrally by a rigid plate and shown in Fig. 8 with the uniformly distributed pressure in $0 \leq r \leq a$

$$q_i = \eta \left(\frac{dw_o}{dt}\right) \quad \ldots\ldots\ldots\ldots\ldots\ldots (59)$$

and a line load

$$\bar{q} = \frac{\eta}{\lambda} \frac{K_1(\lambda a)}{K_o(\lambda a)} \left(\frac{dw_o}{dt}\right) \quad \ldots\ldots\ldots\ldots\ldots (60)$$

along the circumference of the plate at r = a.

CIRCULAR RIGID PLATE SUBJECTED TO A CENTRAL LOAD AND MOMENT

The procedure for a circular rigid plate subjected to a central load and moment is as noted in the section headed "Rigid Strip Subjected to a Central Load and Moment" and illustrated in Fig. 9. Here the condition that no tension be created in the contact area is

$$\frac{M}{P} = e \leq \frac{a}{4} \quad \ldots\ldots\ldots\ldots\ldots\ldots (61)$$

in which a is the radius of the rigid plate. Here also we assume that the load P and moment M are time independent.

Because the rigid plate loaded centrally has been treated previously it is now possible to solve the problem of the circular rigid plate subjected to a moment as shown in Fig. 14.

The deflections in the region $r \leq a$ for a known α_o are

$$w_i = \alpha_o r \cos \theta \quad \ldots\ldots\ldots\ldots\ldots\ldots (62)$$

and the corresponding pressure distribution is

$$q_i = \eta\, r\, \omega_o \cos\theta \quad \ldots\ldots\ldots\ldots\ldots\ldots (63)$$

in which $\omega_o = d\alpha_o/dt$ is the angular velocity of the rotation. Now the deflection surface outside the rigid plate ($r \geq a$) is not axially symmetric. For its

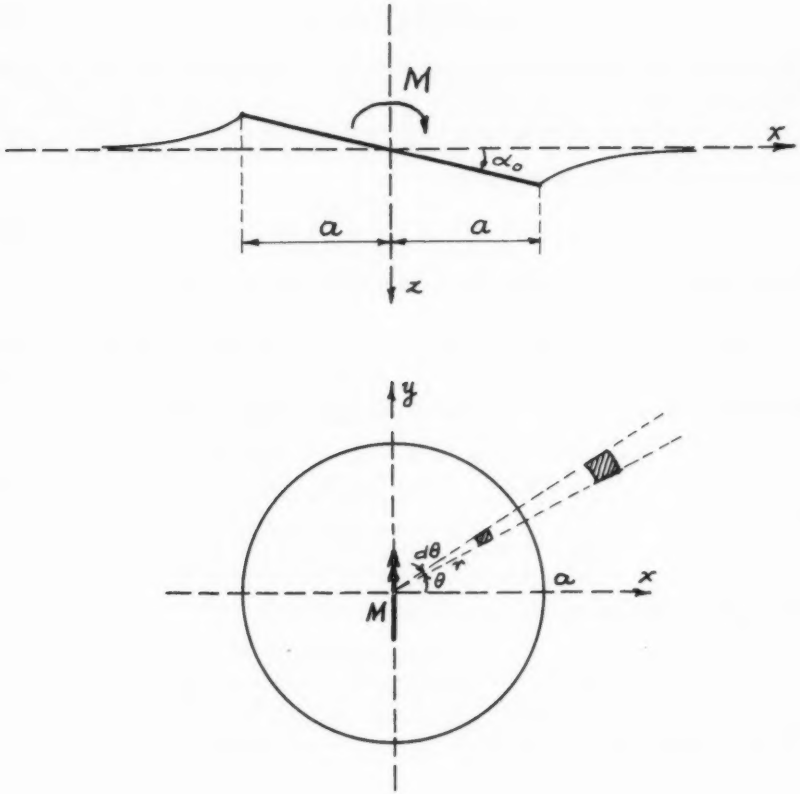

FIG. 14

determination Eq. 7 must be used in the form

$$\frac{\partial^2}{\partial t^2}\left(\frac{\partial^2}{\partial r^2} + \frac{1}{r}\frac{\partial}{\partial r} + \frac{1}{r^2}\frac{\partial^2}{\partial \theta^2} - \lambda^2\right) w = 0 \quad \ldots\ldots\ldots (64)$$

The shape of the deflection surface w_i at $r = a$ suggests that the deflections for $a \geq r$ will be of the form

$$w_e(r, \theta, t) = W(r, t) \cos\theta \quad \ldots\ldots\ldots\ldots\ldots (65)$$

The general solution of Eq. 64 is then

$$w_e(r, \theta, t) = (C_1 + C_2 t)\left[A I_1(\lambda r) + B K_1(\lambda r)\right] \cos \theta \quad \ldots\ldots\ldots (66)$$

in which I_1 and K_1 are modified Bessel functions of the second kind of first order.

Because w_e is expected to be zero at infinity and because at $t = 0$ the deformations due to creep are zero setting $C_2 B = C$ yields

$$w_e = C t K_1(\lambda r) \cos \theta \quad \ldots\ldots\ldots\ldots\ldots\ldots (67)$$

The constant C is determined from the condition that for any t at $r = a$, $w_e = w_i$. Thus

$$w_e = \alpha_o a \frac{K_1(\lambda r)}{K_1(\lambda a)} \cos \theta \quad \ldots\ldots\ldots\ldots (68)$$

and the corresponding pressure is

$$q_e = \eta a \omega_o \frac{K_1(\lambda r)}{K_1(\lambda a)} \cos \theta \quad \ldots\ldots\ldots\ldots (69)$$

Equilibrium of moments about the y-axis (Fig. 14) requires

$$M - \int_0^a \int_0^{2\pi} q_i (r \cos \theta)\, r\, dr\, d\theta - \int_a^\infty \int_0^{2\pi} q_e (r \cos \theta)\, r\, dr\, d\theta = 0 \quad \ldots (70)$$

Substituting Eqs. 63 and 69 into Eq. 70 and integrating yields

$$M = \eta \omega_o \pi a^3 \frac{(\lambda a) K_1(\lambda a) + 4 K_2(\lambda a)}{4 \lambda K_1(\lambda a)} \quad \ldots\ldots\ldots (71)$$

and

$$\omega_o = \frac{4 \lambda a K_1(\lambda a) M}{\eta \pi a^4 \left[\lambda a K_1(\lambda a) + 4 K_2(\lambda a)\right]} \quad \ldots\ldots\ldots (72)$$

The angle of rotation α_o at a time t is then

$$\alpha_o = \frac{4 \lambda a K_1(\lambda a) M t}{\eta \pi a^4 \left[\lambda a K_1(\lambda a) + 4 K_2(\lambda a)\right]} \quad \ldots\ldots\ldots (73)$$

if it is assumed that at $t = 0$ the creep deformation starts.

THE DETERMINATION OF THE CONSTANTS μ AND η

The determination of μ and η can proceed along lines suggested by Pasternak for the elastic case. For the case treated here, namely time dependent deformations, a circular rigid plate of radius a is to be subjected to a constant load eccentrically placed, with an eccentricity $e \leq \frac{a}{4}$. From the time deflection measurements, graphs w_o versus t and α_o versus t are then plotted. The slopes of each graph are (or, rather, should be) the constant values $\left(\frac{dw_o}{dt}\right)$ and $\left(\frac{d\alpha_o}{dt}\right) = \omega_o$ respectively. Substituting them into Eqs. 57 and 72 two equations are obtained from which the values of μ and η can be determined.

This procedure should be used first to prove the applicability of the developed theory for the foundation material under consideration.

In this connection it should be noted that the plate diameter should not have any influence upon the determined material constants. Experiments should also establish the maximum contact pressure for which the time-deflection relation is still (nearly) linear, because this is one of the conditions on which the developed analysis is based.

ACKNOWLEDGMENTS

This paper is part of the consulting activities of the writer for SIPRE. The writer wishes to thank W. K. Boyd, F. ASCE, Chief, Applied Research Branch, SIPRE for helpful comments and A. Assur, Applied Research Branch, SIPRE for a critical review of the manuscript.

APPENDIX I.—NOTATION

The following symbols adopted for use in this paper are listed here for convenience of reference and for the aid of discussers:

A, B, C_1, C_2, C = integration constants;

a = radius of loaded area or circular rigid plate;

$2b$ = width of loaded strip or loaded rigid strip;

e = excentricity of external load;

M = external moment;

P = concentrated external load;

$\overline{P}$ = external line load;

p = distributed external load;

q = vertical pressure of viscous elements upon shear layer;

q_e = vertical pressure outside the loaded region;

q_i = vertical pressure inside the loaded region;

q_o = constant vertical pressure in the region of rigid plate;

$\overline{q}$ = line reaction along edge of rigid plate;

r, θ = polar coordinates in the surface of foundation;

t = time;

w = deflection of foundation surface perpendicular to x, y plane;

w_b = deflection at $x = b$;

w_e = deflection outside the loaded region;

w_i = deflection inside the loaded region;

w_o = constant deflection under rigid plate;

x, y = cartesian coordinates in the surface of foundation;

α_o = angle of rotation of rigid plate;

Δ = Laplace operator;

λ^2 = η/μ ;

ρ, ϕ = auxiliary polar coordinate system;

μ , η = viscous foundation constants; and

ω_o = angular velocity of rigid plate.

APPENDIX II.—SOME PROPERTIES OF THE $K_o(\lambda R)$ - FUNCTION WITH $R^2 = r^2 + \rho^2 - 2r\rho \cos\phi$

According to G. N. Watson[8] with $\nu = 0$

$$K_o(\lambda R) = \sum_{m=-\infty}^{+\infty} K_m(\lambda r)\, I_m(\lambda \rho) \cos m\phi \quad \ldots\ldots\ldots (74)$$

and because of symmetry of Eq. 74 in r and ρ

$$K_o(\lambda R) = \sum_{m=-\infty}^{+\infty} K_m(\lambda \rho)\, I_m(\lambda r) \cos m\phi \quad \ldots\ldots\ldots (75)$$

Multiplying Eqs. 74 and 75 by $d\phi$ then integrating from $\phi = 0$ to $\phi = 2\pi$ and noting that

$$\int_0^{2\pi} \cos(m\phi)\, d\phi = \begin{cases} 0 \text{ for } m \neq 0 & \ldots\ldots\ldots\ldots (76a) \\ 2\pi \text{ for } m = 0 & \ldots\ldots\ldots\ldots (76b) \end{cases}$$

yields

$$\int_0^{2\pi} K_o(\lambda R)\, d\phi = 2\pi\, K_o(\lambda r)\, I_o(\lambda \rho) \qquad \text{for } r > \rho \quad \ldots\ldots (77)$$

$$\int_0^{2\pi} K_o(\lambda R)\, d\phi = 2\pi\, K_o(\lambda \rho)\, I_o(\lambda r) \qquad \text{for } r < \rho \quad \ldots\ldots (78)$$

---

8 "Theory of Bessel Functions," by G. N. Watson, Cambridge Univ. Press, New York, 1945, p. 361, Eq. 8.

Journal of the
ENGINEERING MECHANICS DIVISION
Proceedings of the American Society of Civil Engineers

ULTRASONIC EVALUATION OF REINFORCED PLASTICS

By Albert G. H. Dietz,[1] M. ASCE

SYNOPSIS

Reinforced plastics are becoming engineering materials of increasing importance. A critical problem is to determine by nondestructive means both the quality and composition of the material in finished structures.

Bursts of ultrasound ranging from 1.5 megacycles to 2.1 megacycles per sec and of a few microseconds duration were transmitted through plain unreinforced polyester and epoxy castings and through specimens of laminates with 25 plies of 185 glass fiber fabric per 1/2-in. thickness, several thicknesses of laminate ranging from 1/4 in. to 1 in. thick, laminates made with varying amounts of entrained air, and laminates with different finishing treatments applied to the fabric.

Velocity of transmission of the ultrasonic pulses proved to be directly proportional to the ratio of glass to resin; the higher the glass content the higher the velocity. Attenuation of the signal passing through the specimen was proportional to the amount of entrained air, that is, to the soundness of the specimen; the higher the air content the greater the loss in energy of the signal. Finish on the fabric had no consistent effect.

Some tests were made with close coupling by silicone oil and the transducers pressed tightly against the specimen, others were made by transmitting the pulses through an appreciable thickness (1/2 in.) of water. Both methods gave consistent results.

Note.—Discussion open until November, 1961. To extend the closing date one month, a written request must be filed with the Executive Secretary, ASCE. This paper is part of the copyrighted Journal of the Engineering Mechanics Division, Proceedings of the American Society of Civil Engineers, Vol. 87, No. EM 3, June, 1961.

[1] Prof. of Bldg. Engrg.; Dir., Plastics Research Lab., Mass. Inst. of Tech., Cambridge, Mass.

It is tentatively concluded that the method shows promise of providing a nondestructive test for quality and composition of reinforced plastics.

INTRODUCTION

Glass fiber reinforced plastics are being utilized in rapidly increasing amounts for structural applications. In these materials the glass fibers impart most of the strength and the resin acts as both binder and support for the fibers. The structural properties therefore depend on the ratio of glass fiber and resin. The soundness of a reinforced plastic part depends to a large extent on the care taken during fabrication to avoid porosity, because porosity may permit penetration by water or other fluids and this, in turn, may lead to deterioration.

Visual examination of a reinforced plastic part generally cannot reveal the ratio of glass fiber and resin present, nor is such examination a reliable indicator of the quality of the part. Some nondestructive means of determining composition and quality is consequently highly desirable.

Of the various nondestructive means of investigating materials, it appears that propagation of ultrasound is one of the most promising for the examination of reinforced plastics. Because the velocity of transmission of a sonic pulse through glass is higher than through the polymeric binder, increasing glass content in a specimen should result in increasing velocity of transmission. A pulse passing through a porous specimen containing air bubbles should be scattered internally and its energy considerably attenuated as compared with a pulse passing through a nonporous specimen. Measurements of time of transmission and of attenuation of pulses of ultrasound should therefore be indicators of composition and quality.

To test this hypothesis, a series of experiments was conducted under the sponsorship of the Naval Ordnance Laboratory, White Oak, Maryland. All specimens were prepared by that agency.

Equipment and Test Procedure.—The equipment used has previously been reported[2,3] and will not be described in detail here. The essential features, shown in Fig. 1, are a rectangular pulse generator that feeds pulses of approximately 5 microsec duration into a barium titanate transducer on one side of the specimen, a similar pickup transducer on the other side, a pulse receiver with attenuator, and an oscilloscope. The shift of the received pulse relative to the transmitted pulse on the time axis of the oscilloscope is a measure of the time of transmission, and the change in the amplitude of the pulse is a measure of attenuation of the signal as it passes through the specimen.

Two types of coupling were used. In the first series of tests the transducers were pressed directly against the sides of the specimens in a film of silicone oil to provide close coupling. In the second series the specimens were immersed in a water cell and the transducers, also immersed in the water cell, were held approximately 1/2 in. away from the sides of the specimens. The water-immersion technique was tried to see if good results could be obtained

2 "A New Tool for Determination of Stage of Polymerization of Thermosetting Polymers," by G. A. Sofer, and E. A. Hauser, Journal of Polymer Science, Vol. VIII, No. 6, June, 1952, p. 611.

3 "Cure of Phenol-Formaldehyde Resin," by G. A. Sofer, and E. A. Hauser, Ind. and Eng. Chemistry, Vol. 45, December, 1953, p. 2743.

with transducers some distance away from the test object. In any practical test this would be much simpler than attempting close coupling with silicone oil.

In the silicone series panel specimens (described subsequently) were first tested dry as received. Panels were then cut in halves, and 1/2 of each panel was immersed in water, heated to 70°C for 1 hr, allowed to cool gradually, and

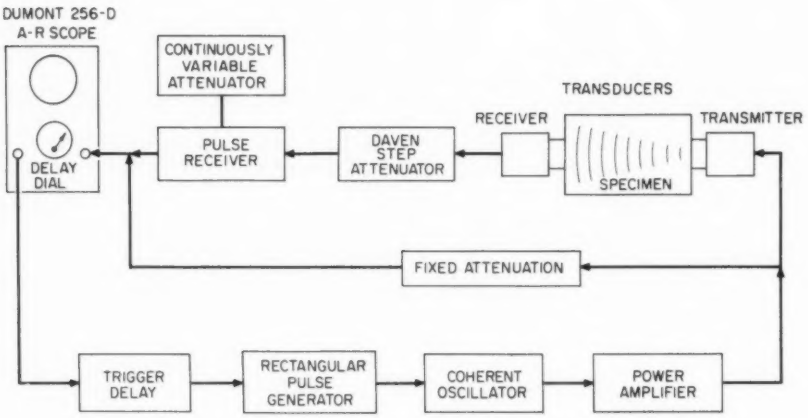

FIG. 1.—FUNCTIONAL BLOCK DIAGRAM OF ULTRASONIC PULSE SYSTEM

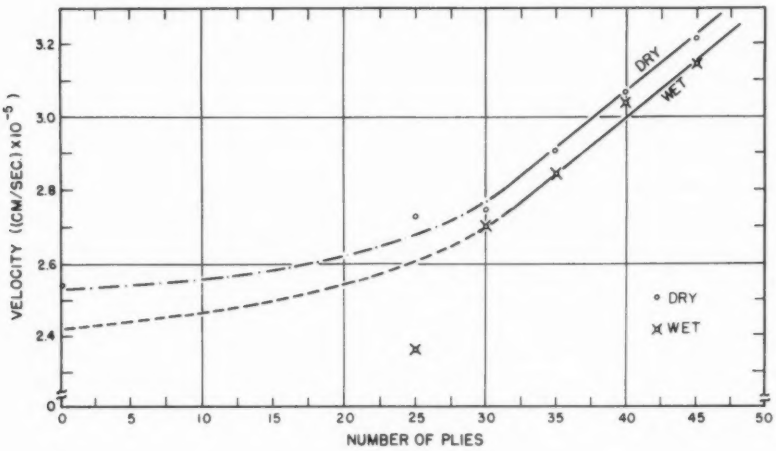

FIG. 2.—ULTRASONIC VELOCITY VERSUS NUMBER OF PLIES, OIL COUPLING

maintained at 24°C, for a total of 48 hr. The objective of this series was to see if moisture pickup would have a detectable effect on the transmission of ultrasound. The other halves of the panels were reserved for tests not pertinent to those reported herein.

TABLE 1.—ATTENUATION AND VELOCITY OF ULTRASONIC CLOSE COUPLING AND WATER IMMERSION

Panel No.	Glass	Finish	Variable	Oil		
				Attenuation		
				Dry		
				Mean	Standard deviation,[b] in %	
(1)	(2)	(3)	(4)	(5)	(6)	
1	25 Plies 182	136	Glass Content	16.6	2.9	
2	30 Plies 182	136	Glass Content	19.0	1.17	
3	35 Plies 182	136	Glass Content	13.1	2.57	
4	40 Plies 182	136	Glass Content	10.3	3.21	
5	45 Plies 182	136	Glass Content	9.1	1.17	
6	18 Plies 182	136	Thickness (1/4 in.)	13.2	4.38	
7	68 Plies 182	136	Thickness (1 in.)	14.0	4.47	
8	35 Plies 182	136	Medium Air	15.5	4.44	
9	35 Plies 182	136	Maximum Air	22.5	4.83	
10	35 Plies 182	Volan	Finish	16.9	2.23	
11	35 Plies 182	112	Finish	13.9	1.61	
12	None	. . .	Polyester Casting	3.9	4.99	
13	None	. . .	Epoxy Casting	7.8	7.97	

[a] $\nu = 2.1 \times 10^6$ cycles per sec

[b] $\frac{\text{Standard Deviation}}{\text{Mean Value}} \times 100 \equiv$ coefficient of variation.

Two sets of frequencies were employed. In the first, a fixed frequency of 2.1×10^6 cycles per sec was used on all specimens. In the second, the frequency was varied from 1.5×10^6 to 2.1×10^6 cycles per sec with certain of the specimens to see if any frequency effects might be noted. This might be particularly noticeable if under some combinations of frequencies and compositions internal standing waves were generated.

Test Specimens.—Specimens were prepared to make possible a determination of the effect of the following factors on ultrasonic transmission:

1. Ratio of resin and glass fabric,
2. Thickness,
3. Air entrainment, and
4. Type of finish employed on the glass fabric. (Because polyester resins do not inherently bond well to glass fibers as manufactured, various types of finishes are applied to the glass to improve the bond.)

Glass fabric employed was type 182.

Finishes employed were those known in the trade as 136, Volan, and 112. Except for the series of panels to test the effect of thickness, all panels were 1/2 in. thick and 6 in. square.

For purposes of comparison, 2 panels of cast resin without reinforcement were included. One consisted of the polyester mix employed in the test specimen and contained 80% of a hard rigid formulation, 15% of a softer more flexible type, and 5% styrene. (Rohm and Hass Paraplex P43 80%, Paraplex P13 15% and Styrene 5%.) The second cast resin panel was a standard epoxy. (Shell Epon 828)

PULSES, GLASS FABRIC-POLYESTER PANELS, SILICONE OIL COUPLING[a]

Coupling (db per cm)		Velocity (10^5 cm per sec)		Water Coupling	
Wet					
Mean	Standard deviation,[b] in %	Dry	Wet	Attenuation (db per cm)	Velocity (10^5 cm per sec)
(7)	(8)	(9)	(10)	(11)	(12)
17.9	1.83	2.73	2.36	19.3	2.52
22.2	1.25	2.75	2.70	19.0	2.71
13.9	3.86	2.90	2.86	14.4	2.84
11.4	3.89	3.06	3.05	13.1	2.97
9.8	2.16	3.21	3.12	11.3	3.11
14.75	3.12	3.01	2.84	18.1	2.87
15.36	1.66	2.86	2.87	14.4	2.80
16.09	1.99	2.94	2.85	16.4	2.83
23.44	3.73	2.89	2.81	22.1	2.83
18.52	5.51	2.95	2.83	16.9	2.83
15.64	2.85	2.97	2.85	15.6	2.83
...	...	2.54	...	...	...
...	...	2.59	...	...	...

Panel characteristics are summarized in Table 1.

Panels 1-5 had glass fabric varying from 25 plies to 45 plies, consequently the ratio of fabric to resin varied but otherwise these panels were identical. Great care was taken to minimize air entrapment. It proved impractical to make good panels with fewer or more plies.

Panels 6 and 7 were 1/4 in. and 1 in. thick. With Panel 3, they constituted a series to measure the effect of thickness.

In panel 9 as much air as possible was deliberately entrapped; in Panel 8 a medium amount of air was added. Panels 8, 9, and 3 (minimum air) constitute a series on air entrapment. It was not possible to determine the actual amount of air contained.

Panel 3 with 136 finish, Panel 10 with Volan, and Panel 11 with 112 finish constitute a series on finishes.

Panels 12 and 13 were cast resins. Panel 12 was the same resin as used in Panels 1 through 11. Panels 12 and 13 afforded comparison between two resins.

Test Results.—

1. Silicone Coupling, Dry and Wet Panels.—Results are summarized in Table 1, columns 5, 6, 7, 8, 9, and 10. Columns 6 and 8 require a little explanation. Standard deviations were computed in the usual manner.

$$S = \sqrt{\frac{(\alpha - \bar{\alpha})^2}{n-1}} \quad \ldots\ldots\ldots\ldots\ldots\ldots (1)$$

in which S is the standard deviation; α represents the individual value; $\bar{\alpha}$ denotes the mean value; and n is the number of observations. To make comparisons

easier, the standard deviations are given as percentage of the mean. This is known as the coefficient of variation.[4]

The salient points are the following:

1. Panels 1 to 5 show that with increasing fabric content there is a decrease in attenuation and an increase in velocity. As shown in Fig. 2, the velocity progression from 45 plies down to about 30 plies is quite linear, but then the dry value deviates to a curve that can be extrapolated to the dry value for zero plies (specimen 12, Table 1, cast polyester) with its value of 2.54×10^5 cm per sec. The wet velocity value for 25 plies deviates from the otherwise regular progression. Because no wet value was obtained for the cast polyester block, the extrapolated curve for the wet condition is only estimated, and shown dotted in Fig. 2. Fig. 3 shows a fairly regular progression of attenuation values, maximum for 25 plies and minimum for 45 plies, except for 30 plies where the values deviate considerably. It is to be noted, moreover, that the attenuation for zero plies (cast polyester) is less than for any of the reinforced panels. This would seem to indicate that a maximum is reached somewhere above zero plies and then attenuation decreases.

Although the wet values in Fig. 2 and 3 depart more markedly from the straight lines than do the dry values, the attenuation values of the wet panels are consistently higher than those of the dry, and the velocity values are consistently lower.

2. Panels 3, 6, and 7 when dry show a regular progression of attenuation with thickness. This is brought out in Fig. 4, in which the attenuations are plotted versus thickness and extrapolated to zero thickness. The line passes through zero attenuation, that is, through the origin. The wet values do not lie closely on a straight line, but the best average wet line lies above the dry line, that is, all attenuation values are higher for the wet material than for the dry.

Velocity values are fairly close, indicating that for the given ratio of resin and glass, held reasonably constant in the three thicknesses, the velocity is reasonably constant.

3. Panels 3, 8, and 9 show that with increasing air entrapment there is an increasing attenuation, as is to be expected from the high attenuation of air. Scatter in the dry results is also greater, as indicated in the greater values of standard deviation for greater air entrapment, but scatter shows no consistent trend in wet values. Velocity values remain fairly constant, although lower for wet than for dry materials, indicating that for the given ratio of resin to fabric the velocity is not affected.

4. Panels 3, 10, and 11 show that different finishes affect the attenuation and standard deviations differently, but have little effect upon velocity either wet or dry, for a given ratio of fabric to resin although wet velocities are lower than dry. Volan developed the greatest attenuation, and 136 the least, although it did not differ greatly, when dry, from 112, which in turn had the smallest standard deviation when wet or dry. Finish 136 dry showed somewhat larger standard deviation than Volan. Volan and 112 showed greater increases in attenuation when wet than did 136. Volan when wet developed greater standard deviation than 136 or 112, but all three showed greater standard deviation when wet than dry. No definite conclusions can be reached as to the effect of finishes.

5. Panels 12 and 13 show that the epoxy and the polyester mix develop approximately the same velocities when dry, but attenuation and standard devi-

4 "Statistical Methods in Research and Production," by Davies, Hafner Publishing Co., New York, 3rd Ed., p. 34.

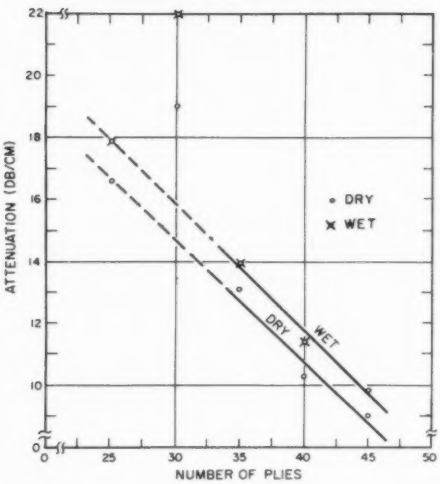

FIG. 3.—ULTRASONIC ATTENUATION VERSUS NUMBER OF PLIES, OIL COUPLING

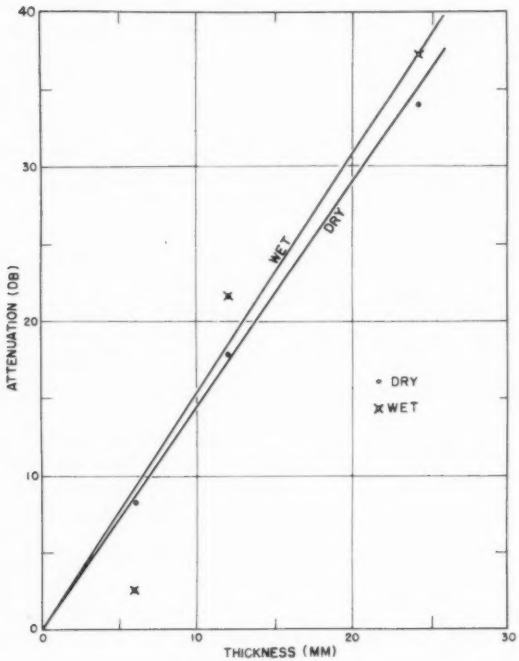

FIG. 4.—ULTRASONIC ATTENUATION VERSUS THICKNESS, OIL COUPLING

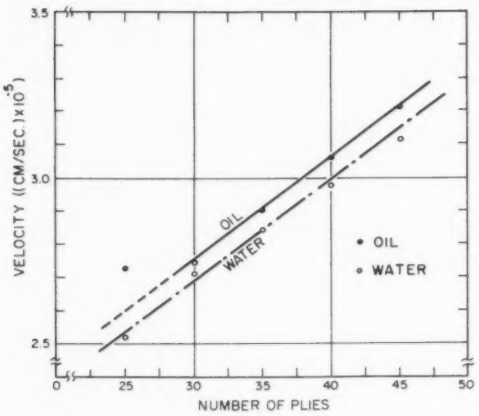

FIG. 5.—ULTRASONIC VELOCITY VERSUS NUMBER OF PLIES, OIL COUPLING

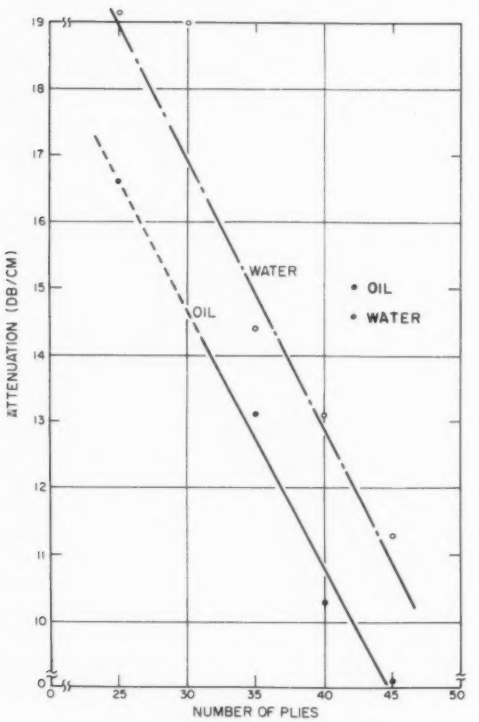

FIG. 6.—ULTRASONIC ATTENUATION VERSUS NUMBER OF PLIES, WATER AND OIL COUPLING

ation of the polyester mix are markedly lower than the epoxy. No wet tests were made.

6. In every instance the attenuation values are higher for the wet panels than for the dry. Velocity values are lower in every instance but one (Panel 7) in which there is no essential change. In Panel 4, likewise, although there is a drop, it is not significant. Velocity changes, in general, are smaller than attenuation changes.

2. Water Coupling, Dry Panel.—Results are summarized in Table 1, columns 11 and 12. These values were obtained by subtracting from the total elapsed time the time needed for the pulse to travel through the water (from known values of velocity of sound in water) and by similarly correcting for the known values of attenuation in water.

One unavoidable source of error was present. The previous tests were made with silicone oil coupling. This oil could not be completely removed even by intensive cleaning. Consequently, perfect wetting of the surface could not be obtained. Imperfect wetting would be expected to lead to higher attenuation values than would occur with good wetting.

Results are summarized in Table 1 and in Figs. 5, 6, and 7. For comparison, corresponding results obtained with oil coupling are included. Fig. 5 gives the velocity values of 25-ply to 45-ply panels and Fig. 6 gives the corresponding attenuation values. Fig. 7 gives attenuation values for 1/4-in., 1/2-in., and 1-in. thick panels.

The salient results are the following:

1. Velocity values in water coupling run slightly lower than in oil coupling. This difference may be real or apparent. It has already been noted that a thin residual silicone oil film made perfect water coupling impossible. It may be that this influenced all readings, including time of propagation of the pulse, and therefore led to apparently reduced velocity values.

2. Although the water-coupling velocities are slightly lower than the oil-coupling velocities, they are consistent and show the same trend as the oil-coupling values. As shown in Fig. 5, the water-coupling velocity values are more consistent than the oil, and the anomaly noted in the 25-ply oil-coupling velocity does not appear in the water-coupling value.

In the various triplets of corresponding panels, that is, Panels 3, 6, and 7; 3, 8, and 9; and 3, 10, and 11 velocity trends in oil and water are similar, and deviations are no greater than the experimental error.

3. Attenuation values in water coupling generally run higher than in oil. It has already been pointed out that this effect may be more apparent than real because of imperfect wetting of the silicone oil-contaminated surfaces of the specimens. The effect may be real if aging has caused degradation of the resin. These panels had aged approximately a year between the time the first tests were run and this series begun. Attenuation is particularly sensitive to the degree of cure of resin as brought elsewhere.[2,3] Degradation might bring about a similar real effect.

4. Although water-coupling attenuation values are higher than oil-coupling, they are consistent in themselves as brought out in Figs. 6 and 7 and in Table 1. In Fig. 6 the 30-ply anomaly previously noted still exists but is less marked in water-coupling than in oil. The fact that the 30-ply attenuations are the same for oil and water is probably a coincidence or an indication that the surfaces of this panel were somehow exceptionally clean of oil. Identical or nearly identical values are also found in some other panels, such as 7, 9, and 10. The ex-

TABLE 2.—ATTENUATION AND VELOCITY OF ULTRASONIC

No.	Glass	Variable	Attenuation (db/cm)					
			Second Series					
			1.5	1.6	1.7	1.8	1.9	2.0
1	25 Plies 182-136	Glass Content	13.3	12.9	13.7	15.8	16.7	19.2
2	30 Plies 182-136	Glass Content	10.7	12.3	13.2	14.9	16.1	17.3
3	35 Plies 182-136	Glass Content	8.6	9.0	10.3	11.5	12.3	13.6
4	40 Plies 182-136	Glass Content	7.3	8.1	8.1	9.4	9.8	10.6
5	45 Plies 182-136	Glass Content	6.1	6.9	7.3	8.1	9.3	10.1
0	P-43 Mix	Casting	5.1	5.9	5.9	6.3	6.3	6.7

[a] $\nu = 1.5 \times 10^6$ to 2.1×10^6 cycles per sec

perimental errors, larger for attenuation than for velocity readings, can also account for apparent coincidences or deviations from the general trend.

5. In Fig. 7 the water-coupling line lies above the oil-coupling line. In water coupling imperfect wetting of the oil-contaminated faces may cause an energy loss at the interface for panels of this glass-resin ratio. This reinforces the suspicion that the increase in water-coupling attenuation values over the oil values is at least largely apparent rather than real.

6. In the various triplets of corresponding Panels 3, 6, and 7; 3, 8, and 9; and 3, 10, and 11, the attenuation trends in water and oil are generally similar, although apparent inconsistencies appear. Most of these are within experimental error. Thus, in 3, 8, and 9, oil-coupling attenuation for 9 is higher than water-coupling, but the difference is smaller than experimental error of approximately ± 0.25 db per cm. The same holds true of the apparently identical attenuation values for oil and water noted in Panel 10.

3. Varying Frequency.—This series was run with water coupling to see if varying frequency would have a noticeable effect on the results. Among these was the possibility that standing waves might occur at certain frequencies and that these would affect the results. Tests were run only on Panels 1 to 5 and the cast polyester panel.

Results are presented in Figs. 8, 9, and 10 and in Table 2. For comparison, the results of the dry tests in the first series of tests are also included in Table 2 in the first two columns headed "First Series, Dry." Fig. 8 shows graphs of velocity versus frequency. Fig. 9 gives attenuation versus frequency. From the velocity values of Fig. 8 the numbers of wavelengths in the thicknesses of the various panels were computed, and in Fig. 10 the attenuation values are replotted against the numbers of wavelengths in the thickness. The higher the velocity the smaller the number of wavelengths in the thickness for a given frequency; consequently, the high glass-content panels, that show the greatest velocity, are shifted to the left in Fig. 10.

The salient results are the following:

1. Velocities are relatively unaffected by frequency, as shown in Fig. 8 and Table 2. Velocity increases with increasing glass content at all frequencies.

PULSES IN GLASS FABRIC POLYSTER PANELS[a]

		Velocity (10^5 cm/sec)							
	First Series, Dry	Second Series							First Series, Dry
2.1	2.1	1.5	1.6	1.7	1.8	1.9	2.0	2.1	2.1
20.4	16.6	2.55	2.57	2.57	2.58	2.57	2.58	2.58	2.73
19.0	19.0	2.63	2.63	2.63	2.63	2.63	2.64	2.64	2.75
15.2	13.1	2.80	2.81	2.79	2.79	2.81	2.80	2.80	2.90
11.8	10.3	2.97	2.99	2.99	2.99	2.97	2.98	2.97	3.06
10.9	9.1	3.05	3.05	3.07	3.06	3.08	3.05	3.08	3.21
6.3	3.9	2.40	2.39	2.39	2.39	2.37	2.39	2.38	2.54

The values obtained in this series of tests are somewhat lower than those obtained in the first series, but are consistent in themselves.

2. Attenuation increases with frequency in all panels and is most marked in the panels having minimum glass content. The cast resin panel shows the least attenuation and the least increase with increasing frequency. For the one frequency common to this series and the earlier series (2.1 megacycles per sec), the attenuation values are somewhat higher in the second series than in the first, but the results are consistent in themselves.

The 25-ply panel shows more erratic results than the others, especially at the lowest frequency. Experimental errors, greatest when making attenuation measurements, may account for this, or the anomaly noted for the 25-ply panel in the first series may again have become noticeable here. The 30-ply panel, that deviated in the first series, shows almost the most consistent results in this series.

3. If standing waves exist, leading to marked reinforcement of signal at half-wave and extinction at quarter-wave and three-quarter intervals, their effect should be brought out in Fig. 10 in which attenuation is plotted versus the number of wavelengths in the thickness of the material. Although some of the plots, notably for the 25-ply and 40-ply panels, show some up and down variations in attenuation, others do not, and the variations that do exist do not appear to be consistent with half-wave and quarter-wave or three-quarter wave intervals, They appear, rather, to be random experimental variations. It does not appear to be possible to correlate the variations with the fabric-resin structure of the panels. No marked variation with wavelength seems to occur in the cast resin panel.

CONCLUSIONS

It is tentatively concluded that

1. Measurements of the rate of propagation and of the attenuation of ultrasonic pulses passed through glass fiber-reinforced polyester panels offer a feasible nondestructive method of determining the proportions of glass fiber

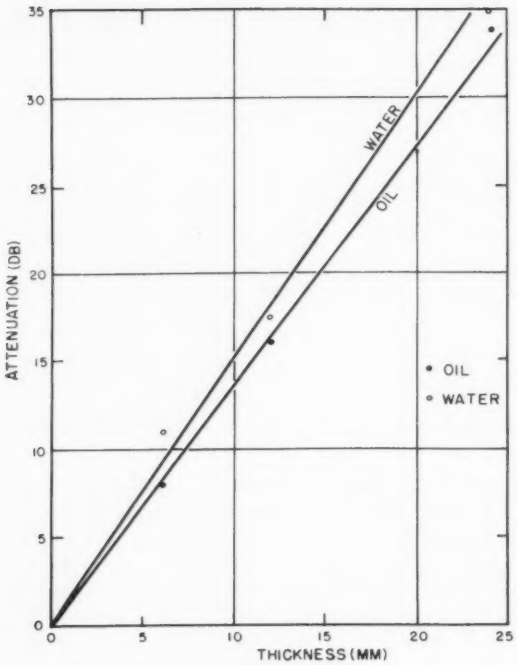

FIG. 7.—ULTRASONIC ATTENUATION VERSUS THICKNESS, WATER AND OIL COUPLING

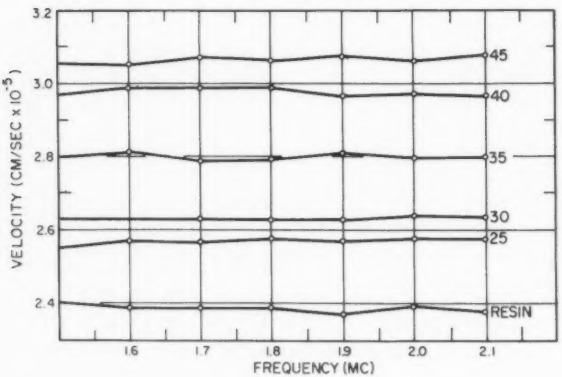

FIG. 8.—ULTRASONIC VELOCITY VERSUS FREQUENCY, WATER COUPLING

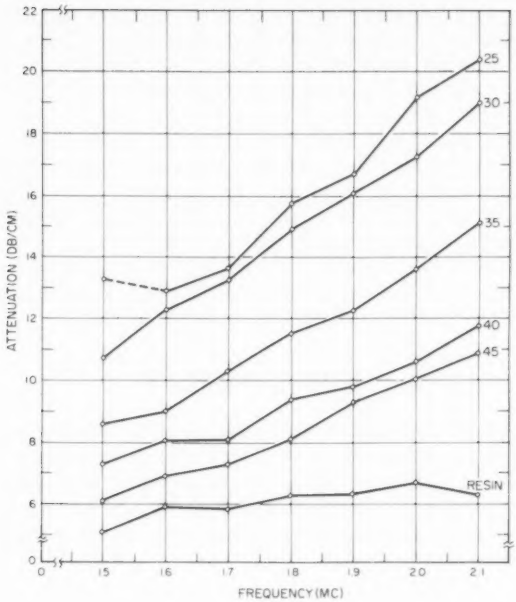

FIG. 9.—ULTRASONIC ATTENUATION VERSUS FREQUENCY, WATER COUPLING

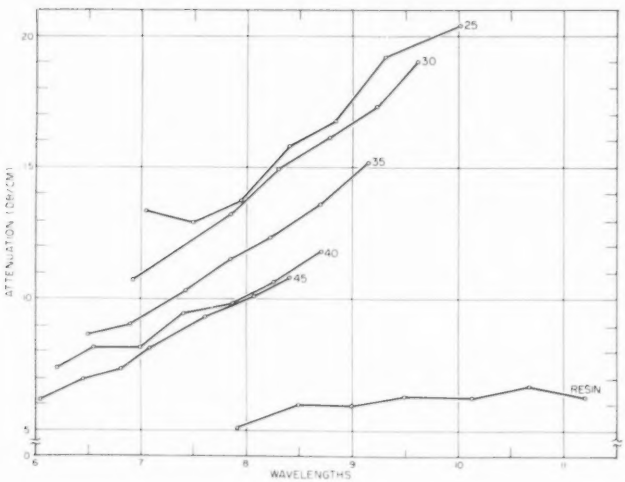

FIG. 10.—ULTRASONIC ATTENUATION VERSUS NUMBER OF WAVELENGTHS, WATER COUPLING

and of resin, and of determining the quality of the laminate, when referred to corresponding standard panels of known composition and quality.

2. Coupling may be satisfactorily accomplished through water layers at least 1/2 in. in thickness, and does not require the use of thin oil films such as silicone.

3. These tests unearthed no evidence that, in the range of frequencies employed, the effect of standing internal waves is of sufficient magnitude to affect the overall trend with respect to velocity and attenuation as affected by composition, quality, and varying frequencies. In this range, velocity is independent of frequency, attenuation is proportional to frequency.

Before the method can be said to be fully established more tests with different compositions, degrees of cure of resin, and with more sets of specimens must be made. The procedure appears to be promising.

ACKNOWLEDGMENTS

These tests were conducted under the sponsorship of the United States Naval Ordnance Lab., White Oak, Md.; H. A. Perry represented the Laboratory and all specimens were prepared under his direction. Jan G. Krizik carried out the tests and performed the computations. F. J. McGarry was helpful with suggestions as the program progressed. The equipment was originally designed and constructed by Milton Cohen.

Journal of the
ENGINEERING MECHANICS DIVISION
Proceedings of the American Society of Civil Engineers

DISCUSSION

Note.—This paper is a part of the copyrighted Journal of the Engineering Mechanics Division, Proceedings of the American Society of Civil Engineers, Vol. 87, No. EM 3, June, 1961.

WHITE NOISE REPRESENTATION OF EARTHQUAKES[a]

Closure by G. N. Bycroft

G. N. BYCROFT.[14]—The approximate derivation of the response spectrum presented by D. E. Hudson, G. W. Housner, and T. K. Caughey is interesting, but the nature of their averaging process is not clear. The equation obtained shows an average oscillation increasing asymptotically with time t_o. In the paper by Hudson, mentioned in their discussion, the time, t_o, is the time duration of the random pulses and therefore should be 25 sec instead of 6.5 sec for the case in question here.

Their sentence that states that the experimental points appear a bit high at the low period end cannot be justified by comparison with an approximate analysis.

The question of using appropriate filters to alter the shape of the power spectral density of the input is a good one. By increasing the energy content towards the low period end of the spectrum, the correspondence between the average earthquake spectra and that of the noise could be made as close as desired. However, as the discussers point out, further statistical comparisons are desirable. Unfortunately, more information than is available is needed to fully substantiate the situation. An indication of the frequency distribution of largest values resulting from a series of bursts of white noise excitation is shown in a further paper.[15] These results show a relatively small dispersion of largest values. The chances of a value greater than twice the average value appear negligible. In fact, approximately 90% of the largest values lie within $\pm 20\%$ of their mean. This is the order of the distribution of actual earthquake spectra about their mean value.

---

[a] April 1960, by G. N. Bycroft (Proc. Paper 2434).

14 Engrg. Physicist, Dept. of Physics, Stanford Research Inst., Menlo Park, Calif.

15 "Effect of Stiffness Taper in Aseismic Design," by G. N. Bycroft, Bulletin, Seis. Soc. of Amer., Vol. 50, No. 4, October, 1960.

BEHAVIOR OF BUCKLED RECTANGULAR PLATES[a]

Closure by Manuel Stein

MANUEL STEIN.[21]—The discussion of the accuracy of the results presented in the subject paper for a plate of infinite length is quite useful. Previous approximate analyses for the infinite plate by Marguerre and Koiter gave appreciably different results from those of the subject paper. It is gratifying to know that an accurate analysis such as that of the discussers gives essentially the same results.

a April 1960, by Manuel Stein (Proc. Paper 2445).
21 Aero Research Engr., Natl. Aero and Space Admin., Langley Field, Va.

BEHAVIOR OF VISCOELASTIC PLATES IN BENDING[a]

Closure by George E. Mase

GEORGE E. MASE.[13]—Some discussion of boundary conditions would certainly have added toward the completeness of the proportional loading solution.

The expression in parenthesis to the right of Eq. 26 was intended to denote the role of α, β, and so on; that is, they were to take on the values of x and y in the moment expressions.

The suggestion of using integral operators because of their close association with the creep function is a good one. Although the concept of solving an elastic plate subjected to a suitable time-dependent load[14] is a convenient one, it was not adopted in this case.

---

a June 1960, by George E. Mase (Proc. Paper 2498).

13 Assoc. Prof. of Applied Mechanics, Michigan State Univ., East Lansing, Mich.

14 "Variational and Lagrangian Methods in Viscoelasticity," by M. A. Biot, I.U.T.A.M., Madrid, 1955.

STRESSES DUE TO THERMAL GRADIENTS IN REACTOR SHIELDINGS[a]

Closure by Melvin L. Baron and Mario G. Salvadori

MELVIN L. BARON,[11] M. ASCE and MARIO G. SALVADORI,[12] F. ASCE.—The restraint method proposed by O. C. Zienkiewicz is particularly interesting whenever solution of the statically indeterminate problem of Stage 3 is already available in the literature or whenever it appears to be easily computable. The Boley procedure used by the writers would presumably be more advantageous whenever the solution of the statically indeterminate problem is cumbersome.

The stress distribution in Fig. 5 refers to the crown of the arch.

The writers are well aware of the fact that, as Zienkiewicz notes, the Duhamel integral presents a powerful tool allowing a solution of numerous thermal problems for the same structure.

Correction.—The authors wish to correct a misprint in Eq. 30. It should read as follows:

$$P = \frac{1}{\gamma}\left[\text{ierfc}(0) - 2\,\text{ierfc}(\gamma) + \text{ierfc}(2\gamma)\right]. \ . \ .$$

[a] June 1960, by Melvin L. Baron and Mario G. Salvadori (Proc. Paper 2516).

[11] Chf. Engr., Paul Weidlinger, Cons. Engrs., New York, N.Y. and Adjunct Prof. of Civ. Engrg., Columbia Univ., New York, N.Y.

[12] Assoc., Paul Weidlinger, Cons., Engrs., New York, N.Y. and Prof. of Civ. Engrg. Columbia Univ., New York, N.Y.

UNDERGROUND STRUCTURES SUBJECTED TO AIR OVERPRESSURE[a]

Closure by Ernest T. Selig, Keith E. McKee, and Eben Vey

ERNEST T. SELIG,[13] A. M. ASCE., KEITH E. McKEE,[14] M. ASCE, and EBEN VEY,[15] F. ASCE.—Regarding the comments by Rongved, the writers fully recognize the complexity of the soil-structure interaction problem for buried structures. The nation's national defense requires the design of such structures today and, hence, an attempt at solving the problem can not "be deferred until well accepted theories of various specific buried structures have been developed." Furthermore such theories are most likely to evolve from a more general approach that is gradually refined as details are considered.

The theory reported in the paper was derived for the case of plane-sided structures, although extensions of this approach to arches, domes, and so forth, have been tried with some success. This theory represents an attempt to present a rational mathematical model that explains arching of the soil over the structure. The soil was not assumed to act as a thick slab, but rather the equilibrium of the mass of soil in the zone of failure was evaluated to determine the forces transmitted to the yielding structure under conditions of impending failure. In a sense, using this approach the soil has been treated as a series of arches. To the extent that this has been done, the paper presents a mathematical statement somewhat analogous to the shell theory outlined by Rongved and having similar "great advantages" and disadvantages.

A number of two-dimensional tests performed by the authors to aid in evaluating the theory have substantiated this approach. Fig. 12 shows the failure planes that formed when a rigid roof panel and a flexible wall panel collapsed under a uniform surface surcharge. Fig. 13 compares the experimental values of uniform, infinite duration overpressure $\bar{p}_\sigma(0)$ required to collapse the roof panel at various depths, H with the theory.

Rongved states that "the dome and shell shaped underground structures induce far more carrying capacity in the overlaying soil than comparable flat-roofed structures." It is difficult to see how Rongved arrives at this. The concept in the "imperfect ditch" theory for tunnels under high fills provides for sufficient deflection over the top of the tunnel to ensure the full benefit of the load carrying capacity of the soil. It seems apparent that without

---

[a] August 1960, by E. T. Selig, K. E. McKee and E. Vey (Proc. Paper 2575).

[13] Assoc. Research Engr., Soil Mechanics Sec., Armour Research Foundation of Illinois Inst. of Tech., Chicago, Ill.

[14] Research Engr., Structural Mechanics Sect., Armour Research Foundation of Illinois Inst. of Tech., Chicago, Ill.

[15] Prof. of Civ. Engrg., Illinois Inst. of Tech. and Supervisor of Soil Mechanics Sect., Armour Research Foundation of Illinois Inst. of Tech., Chicago, Ill.

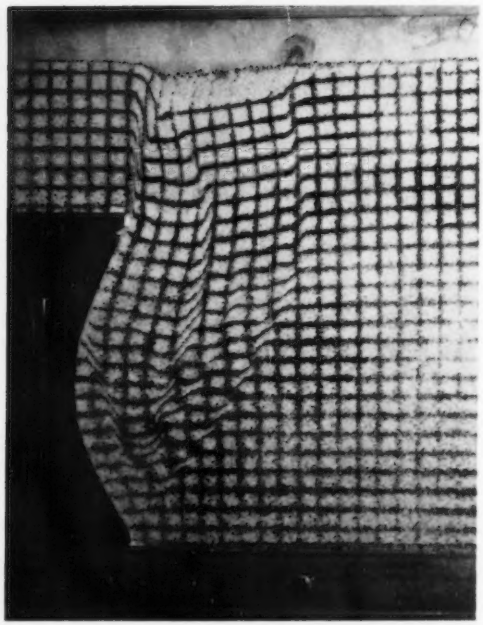

a) Flexible Wall Panel

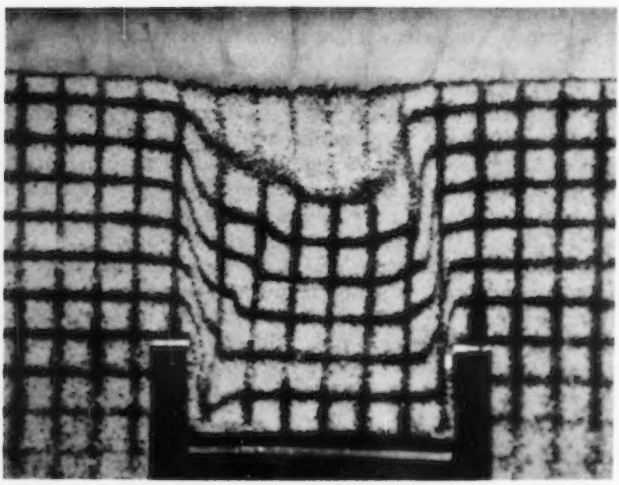

b) Rigid Roof Panel

FIG. 12.—OBSERVED FAILURE OF DRY SAND UNDER UNIFORM SURFACE SURCHARGE

this provision a flat roof would undergo more vertical deflection than a dome and, hence, would permit more load to be carried by the soil.

Kovac and Frankian correctly understand that the structural elements are assumed to have failed and that the soil strength is subsequently determined. The total resistance is then the ultimate strength of the structural element plus the associated soil strength. There was no attempt made in the paper to apply the method of solution to static problems although they should apply.

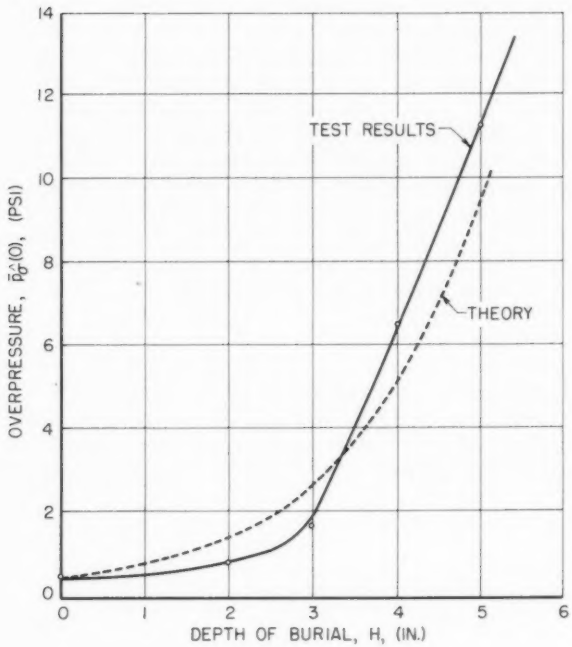

FIG. 13.—COMPARISON OF THEORY WITH TEST RESULTS FOR RIGID PANEL ROOF

It is apparent, however, that a buried structure does not have to support the full weight of soil above it and this fact is recognized in various ways in normal design practice. The ultimate strength of the structural elements were therefore selected to represent what the writers felt was reasonable for normal conditions. Hence, the meaning of the symbol used for ultimate resistance, p_m, is the full resistance of the structural element.

It has not been shown that a limiting depth of burial exists as defined by the discussors, although the pressure required to fail the structure becomes greater at an increasing rate and appears to become infinite at a

finite depth. The theory presented in the paper exhibits this behavior as do the experimental results as shown in Fig. 13. With regard to the soil properties given in Table 1, these were provided as stated in the paper for use if "other information is not available." The comment that this was necessary "so that Eq. 21 would have significance" is incorrect, because for $\phi = 0$, as can easily be observed, Eq. 21 holds and simply becomes

$$E = p_m + H\left[\frac{2c}{L} - \gamma\right] \quad \ldots\ldots\ldots\ldots\ldots \quad (34)$$

ARCH DAM ANALYSIS WITH AN ANALOG COMPUTER[a]

Discussion by Raymond A. Hill

RAYMOND A. HILL,[22] F. ASCE.—No attempt will be made by the writer to criticize or amplify this excellent paper on the application of electric analog computers to arch dam analysis, because the paper describes clearly the advantages and limitations of various methods of analysis. The writer wishes to point out only that preliminary designs must be carried out in much more detail than would be the case if a digital computer were used to analyze the stresses by the trial load method.

On the other hand, it was found in the analysis of Blue Ridge Dam, described by the author, that variations in loading, changes in boundary conditions, and temperature effects could be evaluated easily and rapidly with the analog computer. The primary limitation on the use of an electric analog computer appears to be the difficulty in modifying the circuits to reflect changes in the geometry of the structure. Each such change involves considerable time, and the computer cannot be used for any other work in the meantime.

The writer, who is responsible for the design of Blue Ridge Dam, was initially skeptical of the value of stress analysis using the electric analog computer, but at the end of the work described by the author all skepticism was gone. There remained only the conviction that accurate and reliable results are obtainable economically, provided that the preliminary design is good and that those who operate the computer are highly competent.

---

a August 1960, by R. H. MacNeal, (Proc. Paper 2578).
22 Cons. Engr., Leeds, Hill and Jewett, Los Angeles, Calif.

DYNAMIC RESPONSE OF BEAMS TRAVERSED BY TWO-AXLE LOADS[a]

Discussion by Enno Penno

ENNO PENNO.[13]—The paper gives a very valuable contribution to the computation of dynamic response of beams with special application to simple span highway bridges. The author discusses the validity of his assumptions referring to experiments with single axle load.[7] Experiments with two-axle loads are not yet reported in the literature known to the writer. However, at the Royal Institute of Technology, Stockholm, Sweden, a number of field tests have yielded results that, in spite of imperfect conditions, could give indication of the validity of the theory on bridge structures.

One of the tests was made on a girder bridge with 15.8 m (51.7 ft) span. The loading was a two-axle truck with a total weight of 10.2 metric tons and a speed of 20 km per hr to 70 km per hr (12.4 mph to 43.5 mph). The bridge surface was smooth in one series of tests but had corrugations of 3/4 in.-by-4 in. boards in other cases. The dynamic moments and reactions were computed by equations given by the author. The differential equations were solved numerically by the Runge-Kutta method.

In many cases the magnitude of the dynamic increment of the bending moment at mid-span in tests, 10% to 50%, corresponds with computed values, and the general configuration of the computed "history" curves is similar to that of the actual ones. The absence of higher frequencies in the oscillograph record supports the assumption of the shape of the dynamic deflection curve that, generally speaking, considers only the first mode of vibration. The records of the reactions at supports compared with computations indicate greater influence of higher frequencies, but the magnitude of the dynamic increment can still be predicted by computations within a narrow margin.

The opposite is the case in which "resonant" speeds are considered. As could be expected, the damping of the system can not longer be neglected and reduces considerably the amplitude of vibrations. Tests with "smooth" surfaces too give pooer affinity to the theory owing to deviations from design grade of the top surface on the bridge and the approach.

Acknowledgement.—The research program at the Institution of Structural Engineering and Bridge Building at the Royal Institute of Technology has been under the supervision of G. Wåstlund. A. Hillerborg has been responsible for the test program and the writer has been responsible for the numerical computations. The computer program was prepared by G. Hjerten.

---

a October 1960, by Robert K. Wen (Proc. Paper 2624).

13 Civil Engr., Institution of Structural Engrg. and Bridge Building, Royal Inst. of Tech., Stockholm, Sweden.

BEARING CAPACITY OF FLOATING ICE SHEETS[a]

Discussion by A. Assur

A. ASSUR.[19]—The comprehensive study of the collapse of ice sheets under loads, prepared by the author has been needed for a considerable time. The recent advances in the theoretical treatment of ideally plastic plates have made this possible.

It may be argued that the stress distribution leading to the full plastic bending moment $M_O = f_O h^2/4$ does not correspond to the true stress picture in an ice sheet. For fresh ice and quick loading this argument may hold; however, for prolonged loading and especially for sea ice the plastic moment may very well be a proper idealization.

More serious in its consequences is Meyerhof's assumption in his Eq. 47 that the hydrostatic reaction is confined within the hinge circle. There is no reason why this should be so. Moreover, large scale loading tests by the laboratory with which the writer is associated have shown that a considerable deflection exists at the circumferential hinge until collapse occurs. After this the ice rises at this point and only then is the hydrostatic reaction essentially confined to the hinge circle. Actual breakthrough occurs only with additional loading or after additional time. Meyerhof neglects shearing forces and a reaction imposed on the surrounding ice sheet, which presumably acts as an elastic rather than as a plastic plate.

Meyerhof overestimates the hydrostatic reaction, therefore his resulting radial moments at b are too small.

It is typical for solutions of this type that some of the geometry cannot be predicted but has to be assumed. Meyerhof does not predict the hinge radius b but, incorrectly, assumes it equal to the radius of the deflection dish in the elastic case (b = 3.9 L). This is not supported by tests. The actual circumferential crack should and does occur well within the deflection radius, a fact Meyerhof discusses as proper but neglects in his further derivations. Meyerhof is forced to stipulate b = 3.9 L because he assumed the full hydrostatic reaction within the hinge circle to begin with in Eq. 47. This is an inconsistency that should be corrected in further work on the subject.

There is good reason to assume that the circumferential crack should occur at the place where the elastic theory would predict the maximum radial stresses. It can be shown that the following condition holds for this location:

---

[a] October 1960, by G. G. Meyerhof (Proc. Paper 2627).

[19] Chf., Applied Research Branch, USA Cold Regions Research and Engrg. Lab., Wilmette, Ill.

$$1 - \mu = \frac{\rho\left(\psi' + \psi_r' \frac{\beta' \alpha}{\beta_r' \alpha}\right)}{\psi + \frac{2\psi_r'}{\rho} + \left(\psi_r - \frac{2\psi'}{\rho}\right)\frac{\beta' \alpha}{\beta_r' \alpha}} \quad \ldots\ldots\ldots \quad (96)$$

in which

$$\rho = r/l \quad \ldots\ldots\ldots\ldots\ldots \quad (97a)$$

$$\psi = -\frac{4}{\pi} \text{ kei } \rho \quad \ldots\ldots\ldots\ldots\ldots \quad (97b)$$

$$\psi_r = -\frac{4}{\pi} \text{ ker } \rho \quad \ldots\ldots\ldots\ldots\ldots \quad (97c)$$

and

$$\beta \alpha = 2 \text{ bei } \alpha \quad \ldots\ldots\ldots\ldots\ldots \quad (97d)$$

$$\beta_r \alpha = 2 \text{ ber } \alpha \quad \ldots\ldots\ldots\ldots\ldots \quad (97e)$$

On numerical evaluation $\left(\text{for } \mu = \frac{1}{3}\right)$ it was found that the result can be approximated by

$$\frac{b}{L} = 2.06 + \frac{a}{3L} \quad \ldots\ldots\ldots\ldots\ldots \quad (98)$$

Field tests have shown that Eq. 98 hold quite well. Young's modulus corresponding to L, however, is very small. The location of maximum radial stresses travels towards the center of coordinates with increasing load and longer application of the load.

The definition of L by Eq. 98 is subject to some criticism. This expression is based on the assumption of Hooke's law with a triangular stress distribution in the vertical profile. The plastic analysis, however, is based on a rectangular stress distribution. Assuming furthermore $\mu = \frac{1}{2}$

$$L_p = \sqrt[4]{\frac{E_p h^3}{6K}} \quad \ldots\ldots\ldots\ldots\ldots \quad (99)$$

may have to be substituted for L.

It is interesting to note that A. Johansson presented[20] in 1947 a solution for the collapse of plates on an elastic foundation, based on the concept of yield lines. Johansson gives a rather sketchy derivation, containing errors. The writer, using the same approach, derived the following condition for collapse

$$f_6 = \frac{P_o}{\pi h^2}\left(1 - \frac{1}{3}\left(\frac{\pi}{a}\right)^{1/3} \alpha^{2/3}\right) \quad \ldots\ldots\ldots \quad (100)$$

---

20 "Forsök med armerade betongplatter pa elastiskst underlag," by A. Johansson, 1947, in Swedish. (Experiments on Reinforced Concrete Plates on Our Elastic Foundation), Betong, H. 3.

that can be written also as

$$P_o = \frac{4\pi}{1 - \frac{1}{3}\left(\frac{\pi}{2}\right)^{1/3} \alpha^{2/3}} M_o \quad \ldots\ldots\ldots\ldots \quad (101)$$

in which

$$\alpha = a/L_p$$

This may be compared with the corresponding approximate Eq. 6 of Meyerhof.

On the basis of Johansson's theory one can also predict the location of the circumferential crack as

$$\lambda = \sqrt[3]{\frac{32}{\pi}\,\alpha} \quad \ldots\ldots\ldots\ldots\ldots\ldots \quad (102)$$

in which

$$\lambda = b/L_p$$

This agrees fairly well with Eq. 98 in a given range. For small loading areas the circumferential crack should approach the center rapidly, as is also actually observed.

The "stiffness modulus" to be used in the computation of L_p according to Eq. 99 is very small. A value of 2300 sq tons, for example, was found for sea ice, 25 cm thick.

A further theoretical development along this line shows that the deflection at the circumferential crack (before collapse) should be 3/4 of the maximum deflection at the center, while Meyerhof assumes zero. Actual tests show a considerable deflection at this point although not quite 3/4 of the maximum.

A number of tests also have been made by our laboratory to study the punching of ice under concentrated loading. Meyerhof suggests use of Eq. 36 for this phenomenon. He overestimates, however, the ultimate load, because Eq. 36 completely neglects the horizontal tensile stresses that are created due to bending. We prefer to add the corresponding stress vectors at the radius a + h, using the exact elastic theory for this purpose. This gives a more realistic solution.

Meyerhof quotes approximate equations for the elastic cases. These, primarily introduced by Westergaard, are no longer necessary, because very detailed tables of the Kelvin functions entering the exact solutions are available.[21]

Throughout his paper Meyerhof uses many other approximations even though more precise approaches can be derived. This can easily produce somewhat misleading results.

For example, let us compare the collapse load for a circular area near the edge of a semi-infinite sheet. Meyerhof recommends Eq. 92, expressed in term of the unknown hinge radius b. On the other hand Eq. 55 gives the collapse load for an infinite ice sheet. The ratio of Eq. 55 to Eq. 92 is then a convenient number showing how much smaller the load has to be if it is a located near the edge of an ice sheet.

---

21 "Tables of Kelvin functions and their derivatives, USA, Snow, Ice and Permafrost Research Establishment," by D. E. Nevel, Technical Report 67, 1959.

The ratio r is

$$r = \left(\frac{1}{4} + \frac{1}{0.825\,\pi\left(1 + 6\,\alpha\right)\left(1 - \frac{4}{3}\,\alpha\right)\left(1 - \frac{1}{4}\,\Sigma\right)} \right) \frac{}{} (1 + 0.95\,\Sigma) \quad \ldots (103)$$

with $\Sigma = e/b$

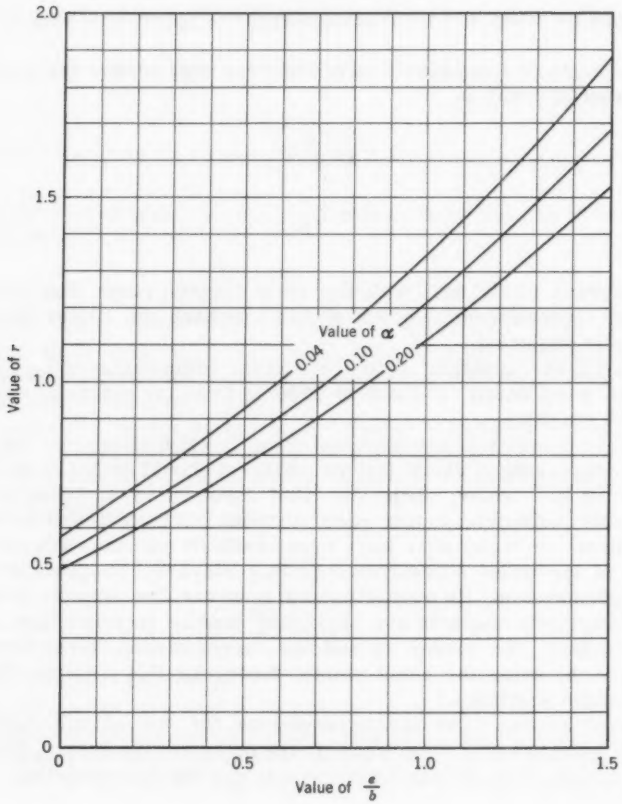

FIG. 12

Fig. 12 shows the results for various α. For small e/b the curves and their first derivatives appear reasonable. The lines should not curve upwards, however, but downwards exponentially approaching unity. The ratio exceeds unity by more than 50% in the region for which Eq. 92 was declared valid. Quite evidently Eq. 92 is not applicable in its present form.

Meyerhof limits his analysis to the discussion of single circular loads or strip loads. For practical purposes it would have been very useful to also discuss the case of two circular loads at various distances (idealized aircraft load) or even four circular loads (wheeled vehicles).

PHYSICAL METALLURGY AND MECHANICAL PROPERTIES OF MATERIALS: BRIHLE FRACTURE[a]

Discussion by H. L. Sujata and Hans Conrad

H. L. SUJATA,[3] A. M. ASCE, AND HANS CONRAD,[4].—In the section Atomic Mechanisms of Cleavage Fracture, the author has emphasized the role dislocations play in yielding and fracture of these materials. While the author has presented the main features of the current thought on this subject, the writers would like to supplement his treatment by elaborating on the relationship between dislocation behavior and the macroscopic stress-strain diagram. Fig. 8 depicts, schematically, the sequence of steps in terms of dislocations that lead to fracture of a typical semi-brittle, dense, fully annealed crystalline solid. (The term semi-brittle is used rather than brittle to distinguish crystalline materials that show some plastic deformation before fracture, although it may be extremely small, from fully brittle materials such as glass.) Shown are the approximate stress ranges in which certain dislocation phenomena have been observed to occur. The phenomena listed in this figure have not been observed completely by any one investigator on a single material, but rather represent a composite of information that has been obtained by a number of researchers on many semi-brittle crystalline materials.[5]

From Fig. 8 it is seen that on application of a stress, the movement of "new" dislocations first occurs (τ_m). These dislocations are so defined because they are not the intrinsic dislocations in the annealed material, but have been generated by scratching or by sprinkling a harder material (such as silicon carbide), on the surface of the specimen.[6,7,8] These new dislocations move more easily than the intrinsic ones that are generally locked by impurity atoms.

As the load is further increased, multiplication occurs and additional dislocations are formed (τ_g) giving slip bands. These dislocations pile up at some obstacle resulting in a stress concentration that is proportional to the

---

[a] December 1960, by B. L. Averbach (Proc. Paper 2686).

[3] Senior Engr., Atomics Internatl., A Div. of North Amer. Aviation, Inc., Canoga Park, Calif.

[4] Senior Tech. Specialist, Atomics Internatl., A Div. of North Amer. Aviation, Inc., Canoga Park, Calif.

[5] "Dislocation Theory Applied to Structural Design Problems in Ceramics," by H. Conrad and H. L. Sujata, paper to be published by the Materials Advisory Bd., Natl. Academy of Sciences, "Symposium, Design with Brittle Materials," December, 1960.

[6] "Dislocation Velocities, Dislocation Densities, and Plastic Flow in Lithium Fluoride Crystals," by J. J. Gilman, W. G. Johnston - Journal Applied Physics Vol. 30, p. 129, (1959). B4a

[7] "Environmental Effects on the Mechanical Properties of Ionic Solids with Particular References to the Joffe Effect," by R. J. Stokes, T. L. Johnston, C.H. Li - Trans-AIME 218, p. 655 (1960). M7n

[8] D. F. Stein and J. R. Low - J. App. Phys. Vol. 31, 362 (1960). B4a

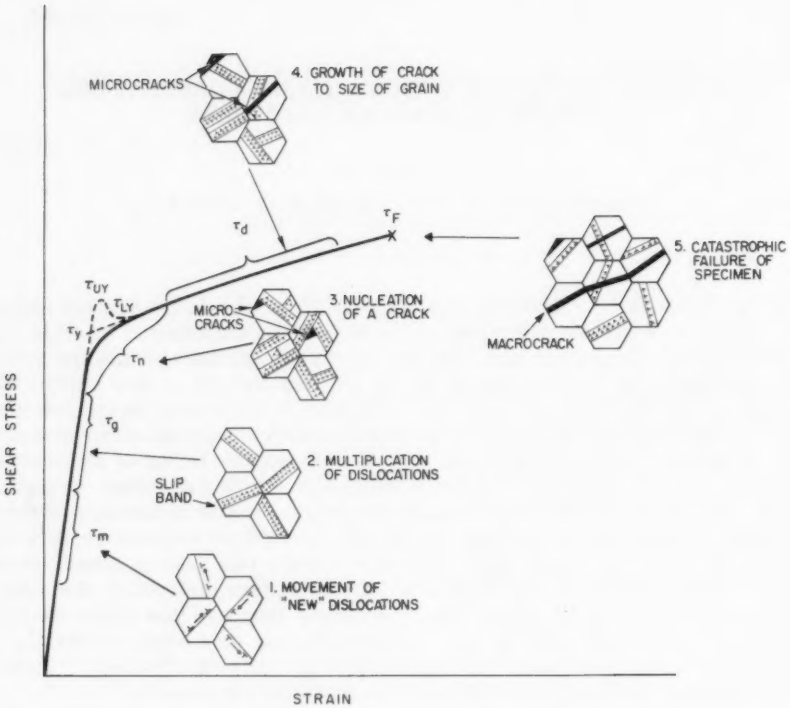

FIG. 8.—SHEMATIC OF THE STEPS LEADING TO FRACTURE OF A SEMI-BRITTLE CRYSTALLINE SOLID IN A TENSION TEST

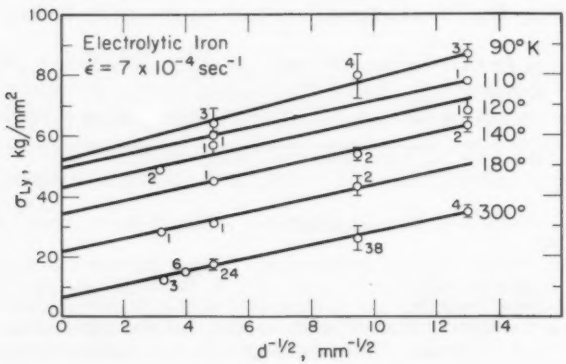

FIG. 9.—EFFECT OF GRAIN SIZE ON THE INITIAL LOWER YIELD STRESS σ_{LY} OF ELECTROLYTIC IRON. (NUMBERS REFER TO NUMBER OF SPECIMENS) (AFTER CONRAD AND SHOECK (5))

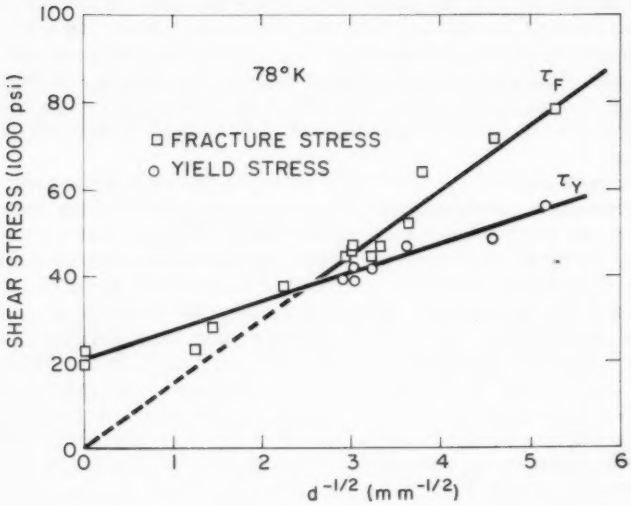

FIG. 10.—EFFECT OF GRAIN SIZE ON THE YIELD AND FRACTURE STRESS OF MILD STEEL @ 78°K (AFTER LOW (6))

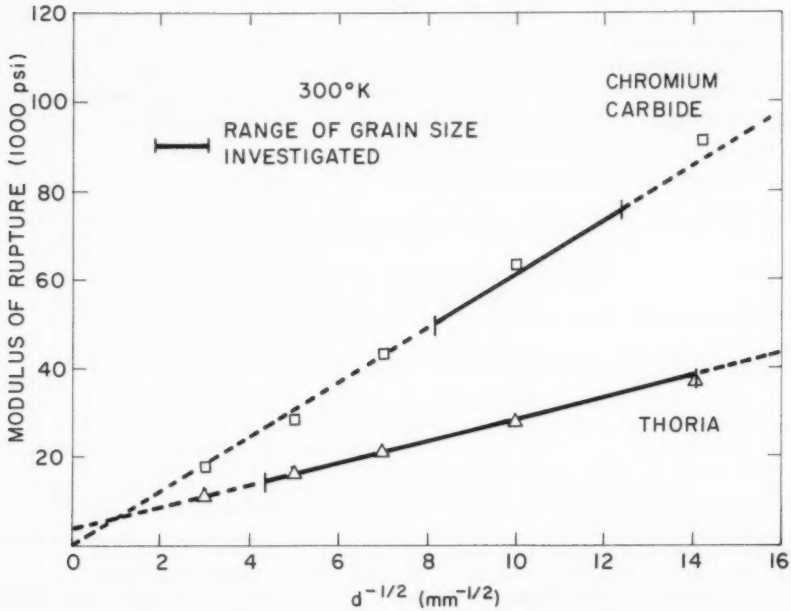

FIG. 11.—EFFECT OF GRAIN SIZE ON THE MODULUS OF RUPTURE OF CHROMIUM CARBIDE AND THORIA (DATE POINTS CALCULATED FROM EQUATIONS BY KNUDSEN (7))

number of dislocations in the pile up. On further increase in stress, the stress level at the head of the pile-up becomes sufficiently large (as a result of the stress concentration) to give yielding (τ_y) and the nucleation of microcracks (τ_n). Because the number of dislocations in the pile-ups is theoretically proportional to the grain size, the effect of grain size on the yield stress given by Eq. 6 is obtained. Experimental verification[9] of this relationship is found in Fig. 9.

In the stress region, τ_d, the crack grows to the size of the grain in which it may, under some circumstances, be temporarily halted before final fracture occurs (τ_f). In the region τ_d to τ_f, the effect of grain size on the fracture stress is given by Eq. 8. Support[10] for this relationship is found in Fig. 10 for mild steel. It is noted from this figure that at large grain sizes (such as small values of $d^{-1/2}$), the fracture stress is equal to the yield stress, whereas at small grain sizes the fracture stress is larger than the yield stress and obeys the Griffith-Orowan relationship, the author's Eq. 2. Some indication that ceramics also obey these fracture relationships[11] is shown in Fig. 11.

It is evident from the preceding that dislocation movement and multiplication play an important role in the behavior of semi-brittle materials. For example, if the dislocations do not move or multiply, fracture can not take place. This information might be useful in selecting a working stress level in design problems. The design methods for semi-brittle materials generally (in 1961) use strength data obtained from modulus of rupture tests. These data are treated in any number of different ways ranging from the simple application of a factor of safety to the modulus of rupture to the more exacting application presented by W. Weibulls.[12] Perhaps another way of obtaining a working stress is to relate it to dislocation movement and multiplication. A working stress level chosen as the stress at which dislocations begin to move or multiply should eliminate the possibility of fracture or failure. These stress levels have not been evaluated (as of 1961) in materials of engineering usefulness and it is recommended that future work be directed toward obtaining such information.

---

9 H. Conrad, G. Shoeck - Acta Met. 8, 791 (1960).

10 "Properties and Microstructure," by J. R. Low - ASM (1954) p. 163.

11 "Dependence of Mechanical Strength of Brittle Polycrystalline Specimens on Porosity and Grain Size," by F. P. Knudsen - J. Amer. Ceramics Soc. 42, 376 (1959). B7c

12 "Statistical Theory of Strength of Materials," by W. Weibull, Ing. Vetenskups Akad. Hand., 1939, No. 151, Ceramics Abstract 1940.

PHYSICAL METALLURGY AND MECHANICAL PROPERTIES OF MATERIALS: FATIGUE OF STRUCTURAL MATERIALS[a]

Discussion by S. K. Ghaswala

S. K. GHASWALA,[14] F. ASCE.—As one interested in and actively connected with the progress and development of aluminium alloys in structural engineering since about 1935, the writer would like to deal with a few salient aspects of fatigue phenomena.

The search for basic knowledge on fatigue that is to discover the mechanism responsible for the formation of cracks, began over a century ago. The progress of this search is evident from the growing mass of symposia and literature that has slowly accumulated in the field (including the field of fatigue behavior of aluminium alloys.[15,16,17,18,19,20,21,22,23] However, in spite of all recorded advances, no satisfactory fundamental theory of fatigue relating the phenomena with the established Natural Laws has been formulated.[24] This was strikingly revealed in the two disasters of the British planes about 1954, when Comet I aircraft G-ALYP met with an accident at Elba, and Comet G-ALYY crashed near Naples. A Court of Inquiry was appointed to go into the details of this accident. One of the three Assessors was W. J. Duncan, who carefully reviewed the causes of failure and gave an admirable survey of the gaps in our extant knowledge on the subject.[25]

According to Duncan one of the unexplained phenomena of fatigue in metals is size effect, observed in light of the fact that the fatigue strengths of geometrically similar specimens of the same metal are not proportional to their

---

[a] December 1960, by Horace J. Grover (Proc. Paper 2688).

14 Cons. Engr., Bombay, India.

15 "Mecanique Industrielle," by J. V. Ponçelet, 2nd Ed., 1839.

16 "Resistance des Materiaux," by A. Morin, 1853.

17 "Internal Stresses and Fatigue in Metals," edited by G. M. Rassweiler and W. L. Grube, D. Van Nostrand, N.Y., 1959.

18 "Fatigue in Aircraft Structures," by A. M. Freudenthal, Academic Press, N.Y., 1956.

19 "Metal Fatigue," edited by J. A. Pope, Ch. and Hall, London, 1959.

20 "Fatigue of Metals and Structures," edited by H. J. Grover, S. A. Gordon, and L. R. Jackson, Thames and Hudson, London, 1956.

21 "Bibliography on the Fatigue of Aluminium Alloys," by B. D. Jones, (contains over 480 references), Aluminium Dev. Assoc., London Tech. Memo 147.

22 "Fatigue, a Bibliography," by J. L. Erickson, Light Metal Age, November, 1945, p. 39.

23 "Fatiuge of Aluminium," by R. L. Templin, (contains nearly 500 references), Proceedings, ASTM, Vol. 54, 1954, p. 641.

24 "Some Aspects of the Plastic Design of Aluminium Structures," by S. K. Ghaswala, Int. Assoc. for Bridge and St. Engrg. Pub., Zurich. Vol. 16, 1956, p. 231.

25 "The Comet and Design against Failure," by W. J. Duncan, Engineering, February 18, 1955, p. 196.

cross sectional areas—the safe stress actually being reduced with increase in linear dimensions.

The phenomena of stress concentration, or as it could be rightly referred to "stress intensification," as suggested by Duncan, plays a significant part in fatigue and plasticity of metals. In the case of aluminium alloys and some other metals which do not have a well defined yield point the plastic flow when stressed beyond the elastic limit permits the relief of high stress concentrations at the highest points. However, in adjacent regions the stress increases. This peculiar phenomena requires detailed study as it could be profitably put to use in applications of a special nature.

As far as this writer is able to discern, this redistribution of stresses may cause the entire member to be more uniformly stressed. Dependent on the nature of loading and intensity, and type of material used, it can be said that a slight amount of plastic deformation is capable of relieving appreciable stresses. The result of plastic deformation in a member having holes and cutouts or any other form of stress raisers, influences its behavior under repeated loading and may increase its fatigue life considerably. The overall design of complex structures for fluctuating loads therefore assumes complications unlike steel where a definite fatigue limit exists.

Stated in engineering parlance as understood by civil engineers, aluminium alloys display differing fatigue properties with differing alloys and strength. In high-strength alloys there is not much difference in the basic fatigue properties of alloys of the type of Duralumin and the Al-Zn-Mg-Cu alloys. With medium strength alloys, small modifications in the chemical composition results in appreciable difference in the fatigue strength, although the alloys may have virtually the same tensile strength. Compared with the heat-treatable alloys of aluminium, the Al-Mg group shows a strikingly sharp knee in the fatigue curve and a definite limit in certain cases. In the case of low-strength alloys, including commercial purity aluminium, the fatigue curves tend to flatten at long endurances.

In a typical test using aluminium alloys having tensile strengths ranging from 5.5 to 39 tons per sq in. it was found that the fatigue ratio (ratio of fatigue strength to ultimate tensile strength) ranged from 0.26 to as high as 0.59. A study of these results indicated that for non-heat-treatable alloys the fatigue ratio lay in the higher range from 0.45 to 0.59, and could be compared with corresponding ratios for mild steel. On the other hand the fatigue ratio for heat-treated materials was very much lower, indicative of doubtful fatigue limit. These figures were based on an endurance of 50 million cycles, which it must be realized is a comparatively very high figure, because in practice this is equivalent to one cycle per minute for 95 yr, or 20 cycles per hr for 285 yr. Normally 50 loadings (alternating) per working day would build up to only 300,000 loadings in approximately 20 yr.

As a broad generalization it can be said that as the fatigue ratio drops with increase in tensile strength, it becomes obvious that if a structure is designed on a purely static strength basis its fatigue resistance will lessen as the static strength of the material increases. Furthermore for static structures in aluminium which carry dynamic loads, such as bridges, the dynamic-static load ratio would invariably be greater than for a similiar structure in steel, because of the lighter weight of the structure itself. Fatigue problems therefore become more accute. The case of high-strength materials, especially those having a very high ratio of yield stress (or proof stress) to ultimate

stress, requires special mention. At points of stress concentration in such materials—which applies to materials other than aluminium alloys—the only real limit to the stress which may be in the material is the limit of proportionality or the yield stress. In other words it means that the stressing in fatigue of that particular member will be superimposed on a very much higher mean stress in the case of a material having a high yield stress than in one having a low yield stress. As such, apart from fatigue characteristics, the latter will have advantages over the former for many purposes.

The practical aspect of fatigue design in aluminium,[26] has been analysed by considering the superimposition of a reversing stress $\pm F_r$ on a steady stress condition F_S. If F_O is the static failing stress and F, is the fully reversed stress which would cause the member to fail at a given number of cycles, then it can be assumed that in the condition representing failure,

$$\frac{F_r}{F} + \frac{F_s}{F_o} = 1 \quad \ldots\ldots\ldots\ldots\ldots \quad (3)$$

It is therefore essential to keep the sum of the stress ratios below unity while in no case should $F_S + F_r$ exceed the allowable design stress.

The civil engineer has much to learn from the aeronautical designer since an aircraft forms one of the most useful and time-tried indices of gaging and solving fatigue problems. This is evident from the fact that during some 40 yr of failure investigation by C. W. George,[27] over 75% of the specimens examined failed by fatigue, giving a crystal clear indication of the importance of this phenomena.

Thus, the methods of providing fatigue safety in aluminium includes the adoption of rational engineering principles by avoiding stress raisers, and gaging, as best as possible, the actual alternating loading which would come on the structure during its lifetime. No amount of theory can supplement the simple fact that absence of a small stress raiser is far more important than mere strength, and that a simple butt weld is superior in fatigue to the same weld heavily reinforced by a splice plate or a rib.

26 "The Strength of Aluminium," Aluminium Co. of Canada Ltd., 1960.
27 Journal Birm Met. Soc. Vol. 27, 1947, p. 308.

ELASTO-PLASTIC ANALYSIS BY NUMERICAL PROCEDURES[a]

Discussion by Le-Wu Lu

LE-WU LU,[8] A. M. ASCE.—The author has developed some useful methods for determining the deformations of partially plastic beams and the ultimate strength of eccentrically loaded columns of aluminum alloy. In a recent investigation[9] on inelastic instability of frameworks, the writer has adopted the numerical integration technique devised by von Kármán[10] (that is also the basis of the scheme shown in Table 1 of the paper) to study similar problems.

To determine the deformation of a simply supported beam subjected to elasto-plastic loading, it is only necessary to perform a series of direct integrations, segment by segment, using the predetermined moment-curvature ($M - \phi$) relationship of the cross section. For the particular type of stress-strain diagram assumed by the author, the $M - \phi$ relationship may be obtained as follows: dividing both sides of Eq. 5 by the yield moment M_y, that is equal to $E_1 I/r_y$ or $E_1 I \phi_y$, and rearranging terms result in the expression

$$\frac{M}{M_y} = (1 - \mu)\left[\frac{3}{2} - \frac{1}{2}\left(\frac{\phi_y}{\phi}\right)^2\right] + \frac{\phi}{\phi_y}\,\mu \quad \ldots\ldots\ldots (22)$$

$$\text{for } 1 < \phi/\phi_y < \infty$$

Eq. 22 can be used to solve for M/M_y corresponding to various assumed values of ϕ/ϕ_y. Results of computation for three B values are shown in Fig. 16. Using these non-dimensional $M - \phi$ curves the deflected shape of the beam of Example 1 can be obtained by integration, starting from the center of the span in which the slope is known to be zero. The integration procedure is similar to that illustrated in Fig. 13. In Fig. 17 the center deflections thus determined are plotted as the dot-dashed line against the integration interval λ chosen in the computations. (This is to study the influence of λ on the accuracy of the results.) The corresponding deflections obtained by Newmark's procedure, that was adopted by the author, are shown as the dashed line. From this figure, the following may be observed:

1. The integration interval λ has considerable influence on the results obtained.

2. Newmark's procedure yields an upper bound to the true deflection. The reason for this is that the formulas used to estimate the equivalent concen-

---

[a] December 1960, by Annabel L. Tong (Proc. Paper 2690).

[8] Research Assoc., Fritz Engrg., Lab., Lehigh Univ., Bethlehem, Pa.

[9] "Stability of Elastic and Partially Plastic Frames," by Le-Wu Lu, Thesis presented to Lehigh Univ. at Bethlehem, Pa. in 1960 in partial fulfillment of the requirements for the degree of Doctor of Philosophy.

[10] "Untersuchungen Uber Knickfestigkeit," by Th. v. Kármán, Forschungsarbeiten, No. 81, Berlin, 1910.

trated loads in such procedure usually would give higher values for cases in which the M/E I diagram has sharp variations.

3. The method of direct integtation always leads to a lower bound to the actual deflection. This is probably due to the under-estimation of the average curvature for each segment.

Thus by averaging the results obtained from these two procedures, a better estimation of the deflected shape can be achieved. The solid line of Fig. 17 shows the average center deflection of the beam under consideration. It may be noticed that even with $\lambda = 6$ in. the center deflection can be determined by averaging the upper and lower bounds of the solutions to within 6% of accuracy.

Referring to the problem of instability of eccentrically loaded columns, the author's approach seems to be similar to that developed by von Kármán and discussed by Timoshenko.[5] In such an approach a set of column deflection

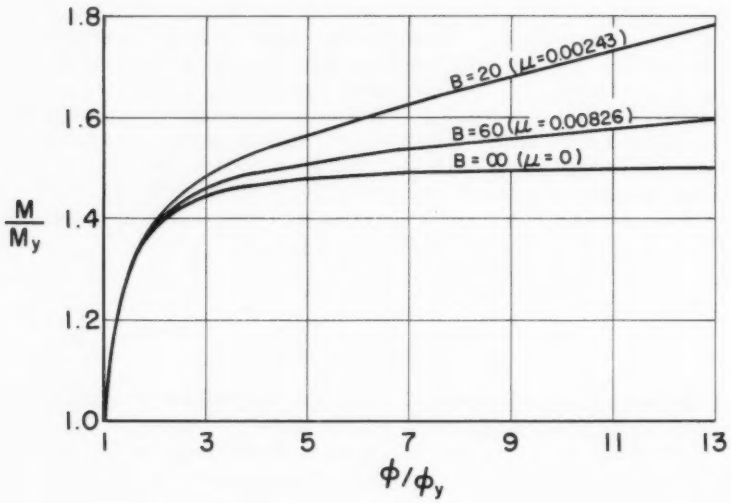

FIG. 16.—INELASTIC MOMENT-CURVATURE RELATIONSHIPS

curves is first constructed for a specified value of the axial force P. Each curve corresponds to a particular value of Δ, the difference between the unit elongation of the two extreme fibers of the mid-height section. The critical length of a column can then be determined by the graphical method indicated in Fig. 15. Morris Ojalvo[11] M. ASCE has developed a more systematic method for determining the critical length of steel columns, in which each column deflection curve is constructed for a specific value of the initial slope (see Fig. 18). In the following an illustrative example chosen from

11 "Restrained Columns," by Morris Ojalvo, Proceedings, ASCE, Vol. 86, No. 5, October, 1960.

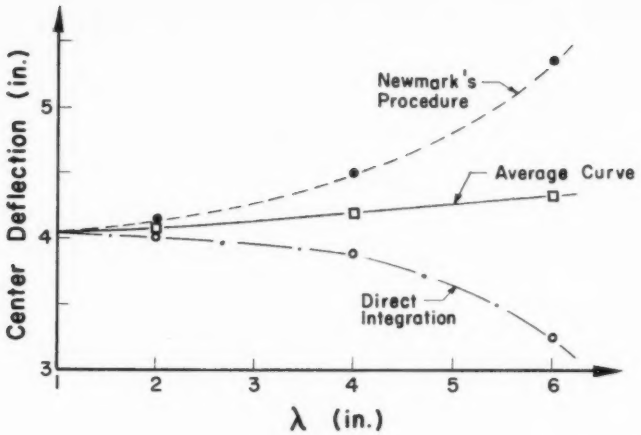

FIG. 17.—COMPARISON OF RESULTS

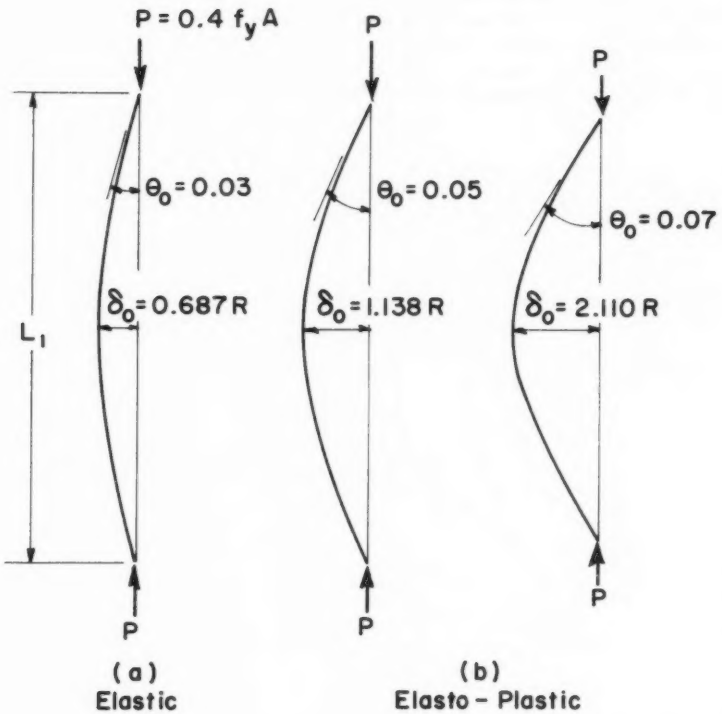

FIG. 18.—COLUMN DEFLECTION CURVES

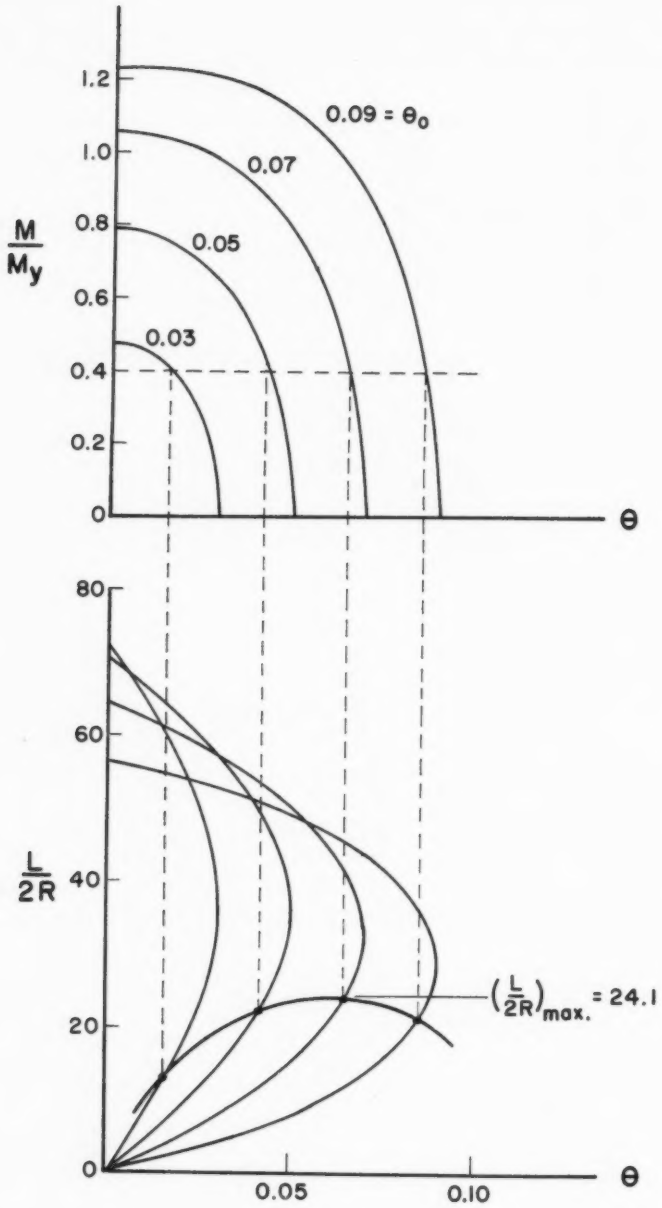

FIG. 19.—NOMOGRAPHS FOR DETERMINING MAXIMUM COLUMN LENGTH

Fig. 6 will be described to show the manner in which Ojalvo's method can be applied to columns of aluminum alloy. The particular problem selected is as follows.

Given: (1) Axial force $P = 0.4\ f_y\ A$, in which A is the cross sectional area of a rectangular column; (2) Eccentricity $\epsilon = 1.0\ R^2/c$. This corresponds to an end moment of $M/M_y = 0.4$. (3) The stress-strain diagram of the material is as shown in Fig. 5.

Required: The maximum column length that is in stable equilibrium with the applied axial force and the end moment.

The non-dimensional $M - \Delta$ diagram of Fig. 12 may be interpreted as the $M - \phi$ diagram of the column member if the scale used for the abscissa is reduced by half (because $\Delta/e_y = 2\phi/\phi_y$. The curve corresponding to $\bar{f}/f_y = 0.4$ can then be used to construct the required column deflection curves by the numerical integration procedure (Table 1), starting from an initial point in which the slope is equal to θ_o. Several such curves are shown in Fig. 18. The information from these column deflection curves is then organized as shown in Fig. 19. In the upper portion the moment at a point on the column curve is plotted against the value of the slope θ at that point. In the lower section the distance of the point on the column curve from the mid-height (non-dimensionalized as L/2R) is plotted against θ. A horizontal line in the upper portion is drawn at the specified moment value. Intersections with the $M - \theta$ curves are carried down to the corresponding curves in the lower section. This determines the equilibrium lengths for the selected column configurations. The longest length found gives the solution. For the present problem the maximum slenderness ratio is equal to 48.2. It may be seen from Fig. 6 that this value of L/R is in agreement with the author's result.

WIND INDUCED VIBRATIONS IN ANTENNA MEMBERS[a]

Discussion by Glenn B. Woodruff

GLENN B. WOODRUFF,[3] ASCE.—Reliable data for the von Kármán coefficient are needed not only for antenna members but also for larger construction such as stacks and refinery vessels. It is to be hoped that the author continue his experiments and furnish such data through the entire range up to Reynold's numbers of 10,000,000.

Possibly, the author's presentation would be clarified by a better definition of the two cases, the first in the Reynolds sub-critical range, that of forced vibrations with the rate of vortex sheading governed by the Strouhal number and, the second, that of self induced vibrations with the rate of vortex sheading governed by the natural frequency of the vibrating member. These two cases are well illustrated by Peter Price (23), Fig. 7. It may be noted that in the second case, there is no "critical" velocity.

The author fails to explain the mathematical processes by which he derived his values of C_k. In their analysis of the failure of the Michigan stacks, with an R of 7,000,000, Dickey and Woodruff, (24) assuming a magnification factor of $1/\delta$, checked their assumption of $C_k = 0.66$. If a factor of π/δ were assumed, C_k would become 0.21. This is in close agreement with Ozker and Smith (25), who arrive at the value of large stacks of 0.20. These two investigations indicate that C_k is constant above R = 500,000.

A factor that has received little investigation is that the wind induced amplitudes, rather than reaching a steady state, show a tendency towards beats. This is indicated by the authors Figs. 2(b) and 4(b), Penzien's Fig. 4, Fig. 3 of Ozker and Smith (25) and numerous other oscillograms. F. B. Farquarhson F. ASCE, (26) found that the frequency of wind induced vibrations was consistently less than the natural frequency, the difference increasing with the damping. As against Farquarhsons' observations of lesser frequency under wind, Dockstader, Swiger, and Ireland (27) report, for the Morro Bay unlined stacks, observations confirming the tendency towards beats but a wind-induced frequency of 73 cycles per minute, higher than the natural frequency of 67 cycles per minute.

A further investigation of this matter may show that the response is not as random as is indicated by the author and that, with appreciable damping, the

---

a April 1961, by William Weaver, Jr. (Proc. Paper 2748).

3 Cons. Engr., San Francisco, Calif.

number of impulses applied in phase are not sufficient to reach the magnification factor of π/δ.

The writer suggests a check of the numerical value of $\bar{R}$ in Appendix I.

ADDITIONAL BIOGRAPHICAL REFERENCES

---

23 "Suppression of the Fluid Induced Vibrations of Circular Cylinders," by Peter Price, Proceedings, ASCE, Vol. 82, October, 1956.

24 "The Vibrations of Steel Stacks," by Walter L. Dickey and Glenn B. Woodruff, Transactions, ASCE, Vol. 121, 1956, p. 1054.

25 "Factors Influencing the Dynamic Behavior of Tall Stacks Under the Action of Wind," by Ozker and Smith, Transactions, ASME, Vol. 78, No. 6, August, 1956, p. 1381.

26 "Model Investigations Which Influenced the Design of the New Tacoma Narrows Bridge," by F. B. Farquarhson, Univ. of Washington Experiment Sta., Seattle, Wash., April, 1954.

27 "Resonant Vibrations of Steel Stacks," by Ernest A. Dockstader, William F. Swiger, and Emory Ireland, Transactions, ASCE, Vol. 121, 1956, p. 1088.

ERRATA

Journal of the Engineering Mechanics Division

Proceedings of the American Society of Civil Engineers

"Bending of Plates on a Viscoelastic Foundation" by K. S. Pister and M. L. Williams, October 1960, Proc. Paper 2619.

pp. 36 and 37. In Figs. 2 and 3, change c H to C H.

pp. 41 and 42. In the captions for Figs. 4 through 7, change X to x.

p. 43. In the fourth line below Eq. 42, change Figs. to Eqs.

"Elastic-Plastic Analysis of Transversely Loaded Plates" by John F. Brotchie, October 1960, Proc. Paper 2622.

p. 59. In the line below Eq. 4b delete the superscript 2.

p. 62. In line 1 of paragraph 5 delete the word Since.

p. 64. In the line below Eq. 15 change $H_n( )$ to $H_n^{(1)}( )$.

In the third line below Eq. 15 change $J_0( )^{(1)}$ to $J_0( )$ and change $J_i( )$ to $J_1( )$. In the fourth line below Eq. 15, change $H_i^{(1)}( )$ to $H_1^{(1)}( )$.

p. 66. In Eq. 21, change the term $(1/r^3)\,w''$ to $(1/r^2)\,w''$.

p. 67. In Eq. 31a, change the term w'''' to w_e''''.

pp. 74 and 77. In the captions for Figs. 6 and 8, change V to μ.

p. 76. In Eq. 73, change ν to μ in three places.

p. 78. Rearrange the expression for P_1 as follows:

$$P_1 = -2\pi M_p \Big/ \left[\log_e \frac{r_b}{L} + k\right] = 3.73\, M_p = 0.189\, P_u$$

and for P_2 as follows:

$$P_2 = -4\pi M_p \Big/ \left[\log_e \frac{r_b}{L} + k\right] = 7.46\, M_p = 0.377\, P_u$$

p. 80. Rearrange the expression for P_3 as follows:

$$P_3 = 16\, M_p \Big/ \left[1 - \frac{8\, r_b}{\pi L}\right]^3 = 18.33\, M_p = 0.928\, P_u$$

and for P_4 as follows:

$$P_4 = 16\ M_p \Big/ \left[1 - \frac{2\ r_b}{L}\right] = 19.75\ M_p = P_u$$

p. 88. Eq. 104 should be written as

$$w_e'' = \left(\frac{\epsilon_{er}}{z}\right)_{z = t/2}$$

"Dynamic Response of Beams Traversed by Two-Axle Loads" by Robert K. Wen, October 1960, Proc. Paper 2624.

p. 93. In line 2, delete the parentheses around the words "an infinite number of degrees."

p. 95. In Eq. 3, change the term m_6 to m_b. In Eq. 7, change the term $\bar{f}(t)$ to $f(t)$.

p. 96. In Eq. 9, change Z to z in two places.

p. 101. In line 4 of the seventh full paragraph, change v t/L = 0.55 to v t/L $\tilde{=}$ 0.55.

p. 104. In line 2 of the fifth full paragraph, change the reference number 7 to 8.

p. 105. In line 2 of the last paragraph, delete the word equal.

p. 106. In line 5 of paragraph 4, change the reference number 7 to 8. In line 5 of paragraph 6, change the reference number 12 to 13.

p. 107. In the expression for A_6, in the first line, change the order of appearance of the final parentheses and the subscript j. In the expression for C_3 insert the term Γ just after Σ and before the subscript j.

p. 108. In the first line of Eq. 41, insert a bar over the term ξ_j^3.

In the second line of Eq. 41, insert a parenthesis immediately after the term ξ_k. In the first line of Eq. 42, insert a bar over the term ξ_j^2.

p. 109. In the second line after Eq. 43, insert a bar over the term ξ_k.

In the line above Eq. 45, insert the term η after the word in and before the word are.

p. 110. In the definition of ϵ_j insert the term ϵ immediately after ; and before the subscript j.

p. 111. In the definition of ψ_j insert the term ψ immediately after = and before the word evaluated.

"Bearing Capacity of Floating Ice Sheets" by G. G. Meyerhof, October 1960, Proc. Paper 2627.

p. 114. In Eq. 2, change s_r to L.

p. 116. In the second line below Eq. 7, change 4 = 2.2 L to r = 2.2 L.

p. 117. In Fig. 2b, add the word Semi infinite to the dashed curve and the word Infinite to the solid curve.

p. 118. In Fig. 3a, add "Infinite:" just prior to $R/b \geq 2.7$ on the upper curve.

p. 122. In line 15, change $\sqrt{2a}$ to $\sqrt{2}\,a$.

p. 123. In Eq. 25, change a $\sqrt{2/L}$ to a $\sqrt{2\,/\,L}$.

p. 124. In the first line after Eq. 26, change $2\sqrt{g}\ L$ to $2\sqrt{g\,L}$.

p. 131. In Fig. 8, add "in psi" to the label "Values of f_b."

p. 134, line 3 from bottom, p. 135, line 5 of Eq. 43, and p. 137, first line after Eq. 60b. Change r - b to r = b.

p. 136. In the numerator of Eq. 50c, insert bracket between the terms P and r^2 and another bracket just after the term b^2.

p. 138. In the fourth line after Eq. 62, insert $\leq$ between the terms a/b and 0.2.

Discussion by Morris Ojalvo and Ahmet Cakmak, October 1960, Proc. Paper 2632, of "Behavior of Buckled Rectangular Plate" by Manuel Stein, April 1960, Proc. Paper 2445.

p. 170. In Fig. 16, change Ref. 18 to Ref. 20.

Discussion by R. J. P. Garden, October 1960, Proc. Paper 2632, of "Commentary on Plastic Design in Steel: Deflections," April 1960, Proc. Paper 2454.

p. 176. In the third line above Eq. 1, change θ''_B to θ'_B. In Eq. 1 parentheses should be added immediately before and after the minus sign preceding θ''_B. In Eq. 2, a bracket should be inserted immediately prior to the minus sign preceding θ''_{34}. Just after the same minus sign, a parentheses should be added. The bracket following the term θ''_{34} should be changed to a parentheses.

p. 179. In line 5, change "curvature" to "curved."

"End-Fixity Effect on Vibration and Instability" by Avid Burgreen, December 1960, Proc. Paper 2679.

p. 19. The equation presently denoted as Eq. 11 is actually the first half of Eq. 11, the last part of which was erroneously labeled Eq. 12. The equation for β just above Eq. 13a is to be marked Eq. 12.